Site Characterisation for Geological Storage of Carbon Dioxide: Examples of Potential Sites from the North West Shelf, Australia

Catherine M. Gibson-Poole

B.Sc. (Hons.) Geology – Royal Holloway University of London, UK

M.Sc. Micropalaeontology – University of Southampton, UK

Australian School of Petroleum

The University of Adelaide

This thesis is submitted in fulfilment of the requirements of Doctor of Philosophy in the Faculty of Science, The University of Adelaide

August 2009

CHAPTER 5. CASE STUDY 1: PETREL SUB-BASIN

5.1 INTRODUCTION

Prior to site selection, the GEODISC™ Program undertook a regional characterisation process to assess sites across Australia for their potential for geological storage of CO_2 (Bradshaw *et al.*, 2000). The potential sites, termed Environmentally Sustainable Sites for CO_2 Injection (ESSCI), were assessed in terms of their location logistics, injectivity potential, containment security, likely storage capacity and proximity to existing natural resources. The outcome of the regional characterisation was a ranked listing of potential ESSCIs with the most appropriate parameters for large-scale CO_2 injection (Bradshaw *et al.*, 2000; Bradshaw *et al.*, 2002).

The Plover ESSCI and Sandpiper ESSCI in the offshore Petrel Sub-basin, northwest Australia (UEI 15 and UEI 16 of Bradshaw *et al.*, 2000), were selected to proceed to detailed site-specific characterisation, as they ranked highly in all assessment criteria except location close to a CO_2 source. They were also selected to provide a conceptual site example of a large-scale, open aquifer system involving thick, laterally extensive, relatively homogeneous reservoirs with no defined structural closure, where hydrodynamic, residual and solubility trapping beneath a regional seal will be important components. The Plover ESSCI comprises the Jurassic Plover and Elang formations as the primary CO_2 injection horizon, sealed by the Frigate Formation. The Sandpiper ESSCI occurs stratigraphically above the Frigate Formation, comprising the Early Cretaceous Sandpiper Sandstone as the secondary potential injection horizon, sealed by the regionally extensive Bathurst Island Group. This chapter documents the detailed geological site characterisation undertaken to assess the CO_2 storage potential of the Plover and Sandpiper ESSCIs in the Petrel Sub-basin.

5.2 LOCATION AND GEOLOGICAL SETTING

The Petrel Sub-basin is a northwest-southeast trending rift in the southern Bonaparte Basin, located off the northwestern coast of Australia in the Joseph Bonaparte Gulf (Figure 5.1). It is flanked to the west, south and east by Proterozoic rocks of the Kimberley and Sturt blocks. The northern end of the Petrel Sub-basin is orthogonally overprinted by the younger northeast-trending Malita Graben (Figure 5.1 and Figure 5.2) (Lee & Gunn, 1988; Mory, 1988; O'Brien *et al.*, 1993).

Figure 5.1 Location map of the Petrel Sub-basin, northwest Australia, and surrounding tectonic elements (modified after Lee & Gunn, 1988).

The study area extends from 50 km to 330 km offshore in a northwesterly direction from Cape Hay (Figure 5.3). The water depth ranges from 35 m at Bougainville-1 in the southeast to 135 m at Gull-1 in the northwest. The Jurassic-Cretaceous deep saline formations of the Petrel and Sandpiper ESSCIs occur within the central part of the basin, but pinch out or thin towards the basin margins. The depth to the base Plover Formation (maximum potential injection depth) ranges from 3100 m at Gull-1 in the northwest to 450 m at Bougainville-1 in the southeast. At present, hydrocarbon accumulations are confined to the Carboniferous and Permian strata, with known large discoveries at Petrel and Tern, and small discoveries at Blacktip, Turtle and Barnett. All hydrocarbon discoveries in the sub-basin to date are yet to be commercialised and developed, therefore there is no infrastructure in place at present.

Figure 5.2 Structural cross-sections of the Petrel Sub-basin (modified after Lee & Gunn, 1988).

5.2.1 Structural and Stratigraphic Evolution

The sedimentary succession in the Petrel Sub-basin extends from the Cambrian to Recent. The basin developed initially as an intra-cratonic rift or sag basin in the Cambrian to Ordovician, tilted fragments of which are seen onshore and in the immediate offshore basin (Lee & Gunn, 1988; Colwell & Kennard, 1996; O'Brien *et al.*, 1996). The salt seen in the offshore basin is likely to have been deposited at around Late Ordovician to Silurian times (Lemon & Barnes, 1997). The Petrel Sub-basin *sensu stricto* was initiated as a northwest-trending rift during the Late Devonian (Gunn, 1988; Lee & Gunn, 1988). The gross geometry of the rift is described as a V-shaped opening, which Lee and Gunn (1988) explain as a "scissor-like widening that occurred about a pole at the rift's southern end". The initial sedimentary fill (Late Devonian to Early Carboniferous) forms a highly faulted and structured sequence that is confined between the original bounding faults of the rift. These sediments were draped by the succeeding Late Carboniferous to Tertiary sediments, which are relatively unfaulted in comparison, and which onlap onto the flanking shelves of Proterozoic basement (Figure 5.2) (Lee & Gunn, 1988; Gunn, 1988).

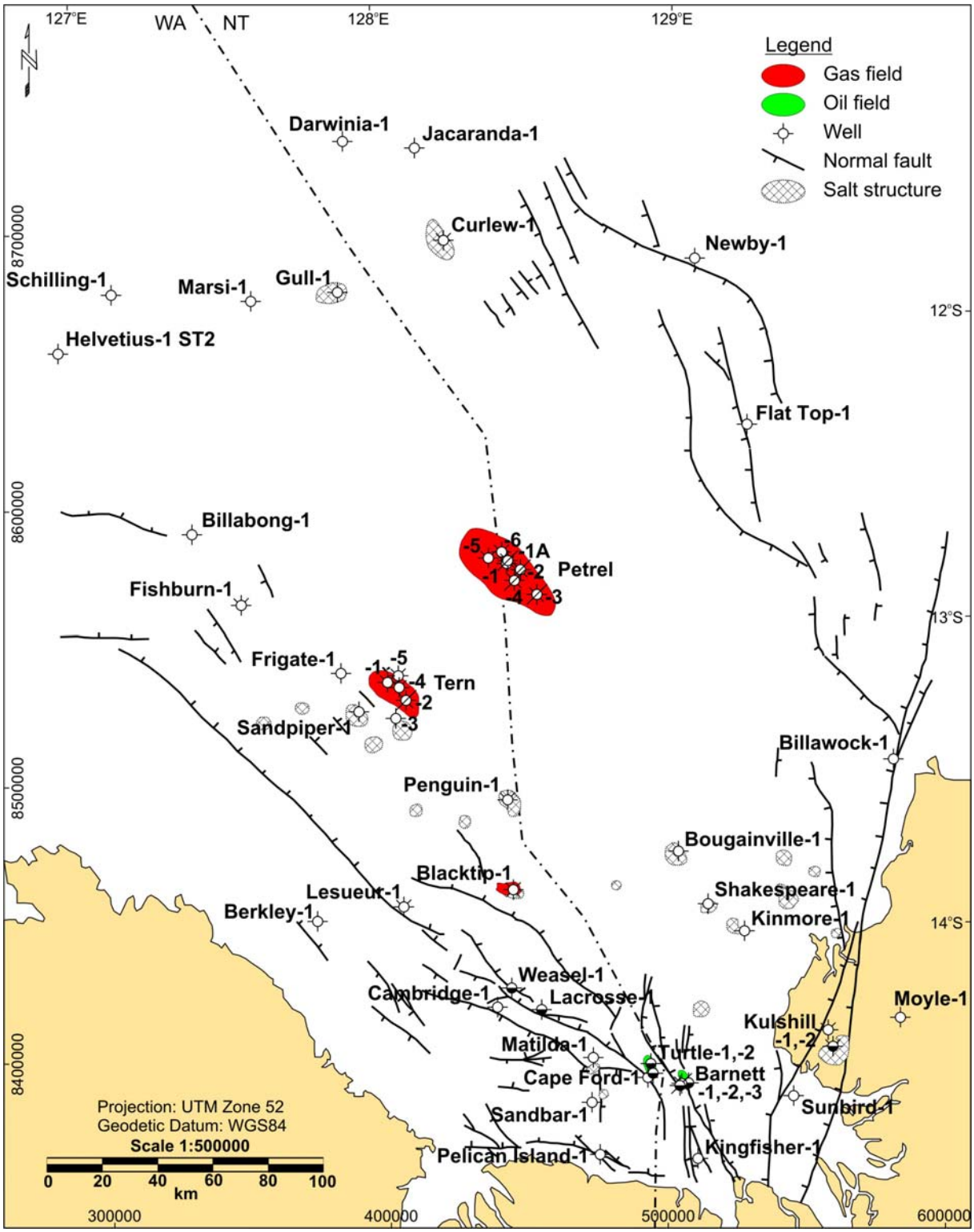

Figure 5.3 Location map of the study area, showing wells, oil and gas fields, salt structures and faults (salt structures and fault traces redrawn after Lee & Gunn, 1988; Colwell & Kennard, 1996).

Following the major rifting and upper-crustal extension in the Late Devonian to earliest Carboniferous, the Carboniferous to Permian became a time of sag-dominated deposition, punctuated by a series of renewed upper and/or lower crustal extension-sag cycles. The sag-

dominated phase was most likely driven by a combination of post-rift thermal cool-down, sediment loading, probable movement on basement faults and/or crustal thinning (Colwell & Kennard, 1996). The crustal extension ceased in the Permian, whereupon thermal subsidence phase sedimentation took over until the Late Triassic (O'Brien *et al.*, 1993). A major compressional reactivation event affected the Petrel Sub-basin during the Late Triassic to Early Jurassic, reactivating faults along the basin margins (mainly in the southwest) (O'Brien *et al.*, 1993; Colwell & Kennard, 1996). The anticlinal structures at the Petrel and Tern fields may have been created by this inversion, although it is also possible that they may have formed as a result of salt movement and progressive salt withdrawal (O'Brien *et al.*, 1993; O'Brien *et al.*, 1996; Lemon & Barnes, 1997). The sediments of the Troughton Group were deposited during the Late Triassic to Middle Jurassic (Figure 5.4). The Malita Formation at the base of the Troughton Group consists of multicoloured 'redbeds', predominantly composed of fine-grained siliciclastics that were deposited in a fluvial depositional environment (Mory, 1988; Colwell & Kennard, 1996). A major period of erosion separates the Malita Formation from the overlying Plover Formation (Colwell & Kennard, 1996).

Post Early Jurassic, the Petrel Sub-basin mainly underwent slow sag, during which time the Plover Formation at the top Troughton Group and the overlying Flamingo Group were deposited (Figure 5.4) (Colwell & Kennard, 1996). The Early to Middle Jurassic Plover Formation consists of extensive, fine to coarse-grained sandstones, with minor amounts shale and coal, deposited in a fluvial-deltaic depositional environment (Mory, 1988; Colwell & Kennard, 1996). By the Middle Jurassic, the northern end of the Petrel Sub-basin became orthogonally overprinted by the northeast-trending tectonic features of the Vulcan Sub-basin, Malita Graben and Sahul Platform (Figure 5.1) (Mory, 1988; O'Brien *et al.*, 1993). The northeast-trending structural features in the Timor Sea region developed primarily as a result of the Late Callovian to Oxfordian continental break-up of Gondwana along the northwestern continental margin of Australia (O'Brien *et al.*, 1993).

The fluvial-dominated sandstones of the Plover Formation are overlain by the more marine-influenced sandstones of the Elang Formation (Figure 5.4) (Arditto, 1996). The Callovian to Oxfordian Elang Formation is of similar lithology to the underlying Plover Formation, but also contains marine shales, glauconite and limestone (Colwell & Kennard, 1996). The depositional environment of the Elang Formation is considered to be coastal plain to nearshore marine (Arditto, 1996). Major fault reactivation that deepened the Sahul Syncline and Malita Graben depocentres to the north resulted in the formation of the regionally recognised Tithonian Unconformity in the Late Jurassic (Labutis *et al.*, 1998).

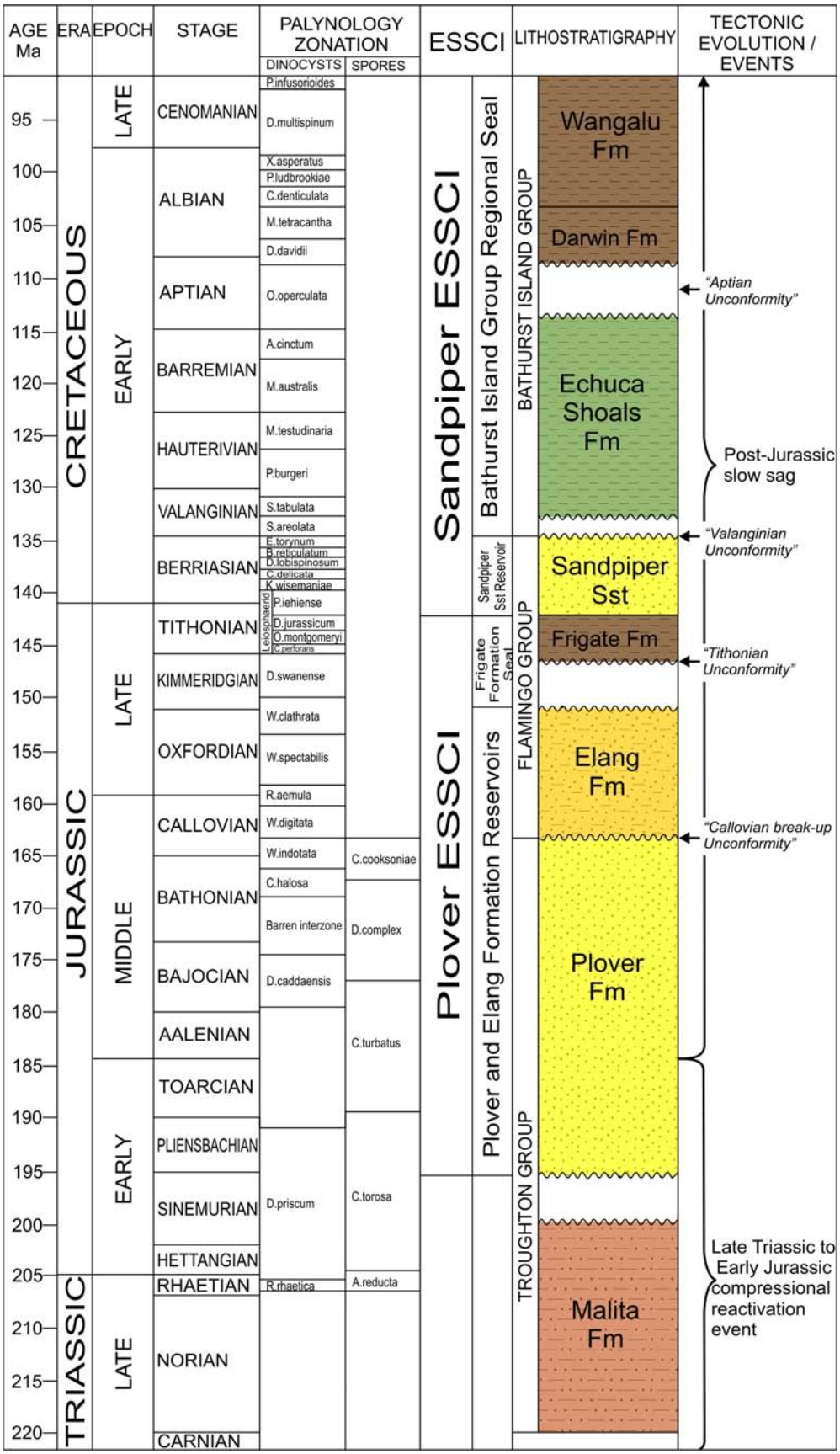

Figure 5.4 Stratigraphic column for part of the Mesozoic succession in the Petrel Sub-basin (modified after Jones *et al.*, 1996). The location of the Plover and Sandpiper ESSCIs in relation to the lithostratigraphic units is indicated.

The overlying Late Jurassic Frigate Formation consists of shale, siltstone and minor fine sandstone and limestone, deposited in a low energy, open shelf environment (Figure 5.4) (Mory, 1988; Colwell & Kennard, 1996). Above the Frigate Formation is the Early Cretaceous Sandpiper Sandstone, which is a thick, fine to coarse-grained sandstone, deposited within a coastal-plain to shallow marginal marine depositional environment (Figure 5.4) (Mory, 1988; Colwell & Kennard, 1996). The final break-up of Gondwana and the separation of India from Australia in the Early Cretaceous produced the regionally recognised Valanginian Unconformity (Botten & Wulff, 1990; Labutis *et al.*, 1998).

Overlying the Flamingo Group and the Valanginian Unconformity is the regionally extensive Bathurst Island Group (Figure 5.2 and Figure 5.4). The Echuca Shoals Formation at the base of the Bathurst Island Group represents the onset of the major Cretaceous marine transgression. It is a highly condensed unit, ranging from Valanginian to Barremian in age, consisting of glauconitic claystones deposited in a shallow marine shelf environment (Botten & Wulff, 1990; Pattillo & Nicholls, 1990; Colwell & Kennard, 1996). At the top of the Echuca Shoals Formation is the Aptian Unconformity, a prominent seismic reflector throughout the Timor Sea area, depicted by an abrupt increase in the silica content of the overlying Darwin Formation. The Aptian to Albian Darwin Formation is a radiolaria-rich claystone unit, deposited in a shallow marine shelf environment (Botten & Wulff, 1990; Young *et al.*, 1995; Colwell & Kennard, 1996; Labutis *et al.*, 1998). The succeeding Wangalu Formation, deposited during Albian to Maastrichtian times, consists of a thick (up to 2000 m) succession of micaceous mudstone with minor marl and limestone that coarsens upwards to siltstone and fine sandstone. The Wangalu Formation is representative of a distal to inner shelf succession (Mory, 1988; Colwell & Kennard, 1996).

Paleocene sandstones and minor carbonates were deposited overlying the Bathurst Island Group in the northern Petrel Sub-basin, before a period of non-deposition across the whole of the sub-basin during the Eocene-Oligocene. Shelf carbonates were re-established across the basin in the Miocene (Lee & Gunn, 1988; Mory, 1988). In the mid-Miocene the Australian continental plate collided with the Indonesian plate along the northern continental boundary, resulting in ENE-WSW compression (Lee & Gunn, 1988; O'Brien *et al.*, 1993).

5.2.2 Pressure, Temperature and Salinity Conditions

The phase state of CO_2 when injected into the subsurface is dependent on the *in situ* pressure and temperature conditions, thus it is necessary to define the pore fluid pressure and

geothermal gradients of the basin. Temperature gradients in the Petrel Sub-basin range from 26.32ºC/km at Petrel-3 to 46.95ºC/km at Curlew-1. The average temperature gradient is 32.81ºC/km (Figure 5.5 and Appendix C). The average hydrostatic pore pressure gradient in the Petrel Sub-basin is 10.00 MPa/km (Figure 5.5 and Appendix B). Based on these gradients, the depth for CO_2 to be in the supercritical phase is about 750 m. Salinity varies from 15000 ppm at Flat Top-1 to 30000 ppm at Sandpiper-1. The average salinity is 24220 ppm.

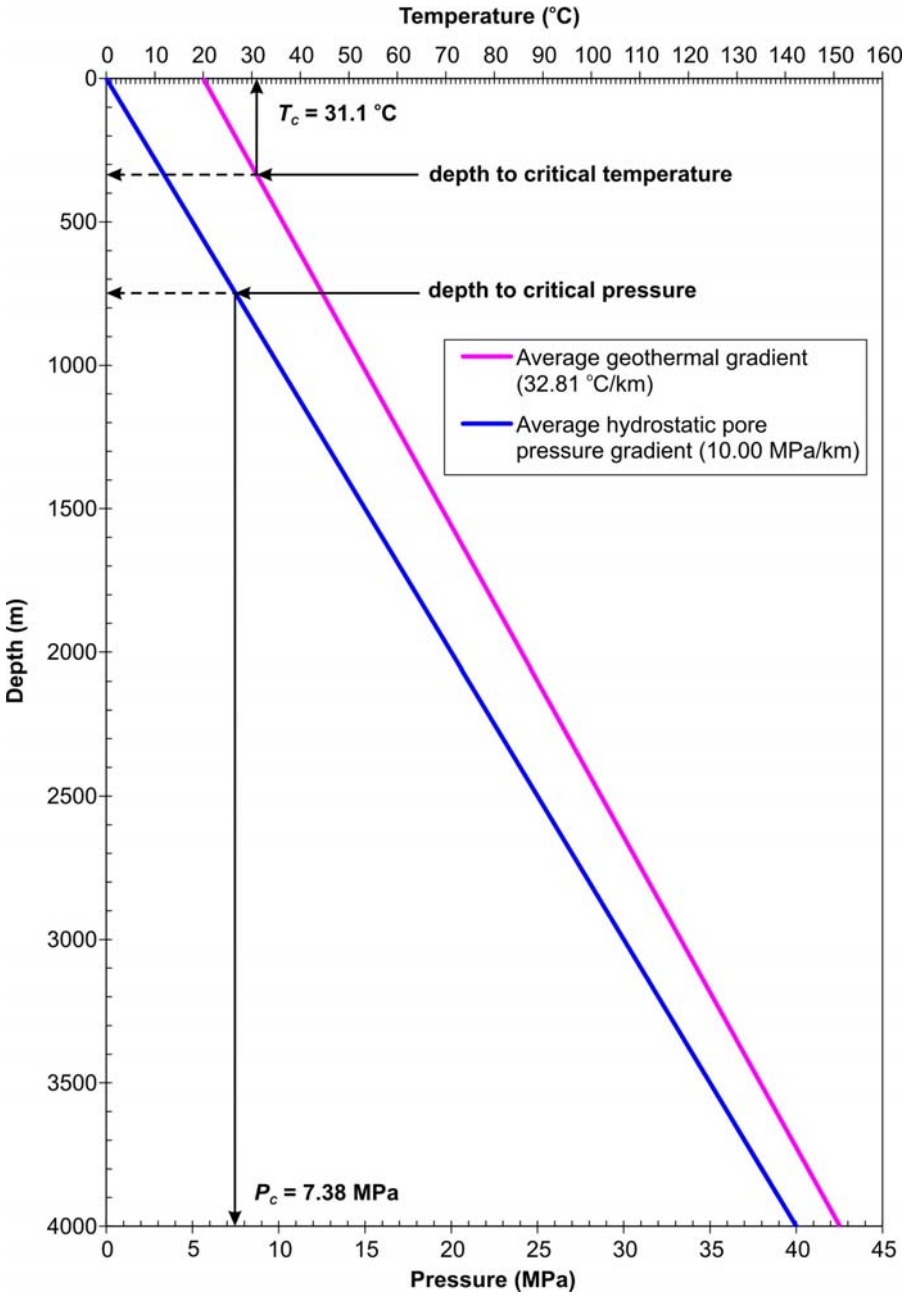

Figure 5.5 Depth to CO_2 critical temperature (T_c) and critical pressure (P_c) in the Petrel Sub-basin.

5.3 METHODOLOGY FOR DETAILED SITE CHARACTERISATION

The methodology for detailed site characterisation was discussed in the previous chapter. A brief summary is provided here, focussing on the geological characterisation aspects that were undertaken for this PhD study (Figure 5.6). Seismic structural and stratigraphic interpretations were integrated with wireline log well correlations, detailed sedimentological core descriptions and biostratigraphy, to develop structural and stratigraphic models for the potential site. These models provided the subsurface framework and formed the basis for the assessment of three principle aspects: injectivity, containment and capacity.

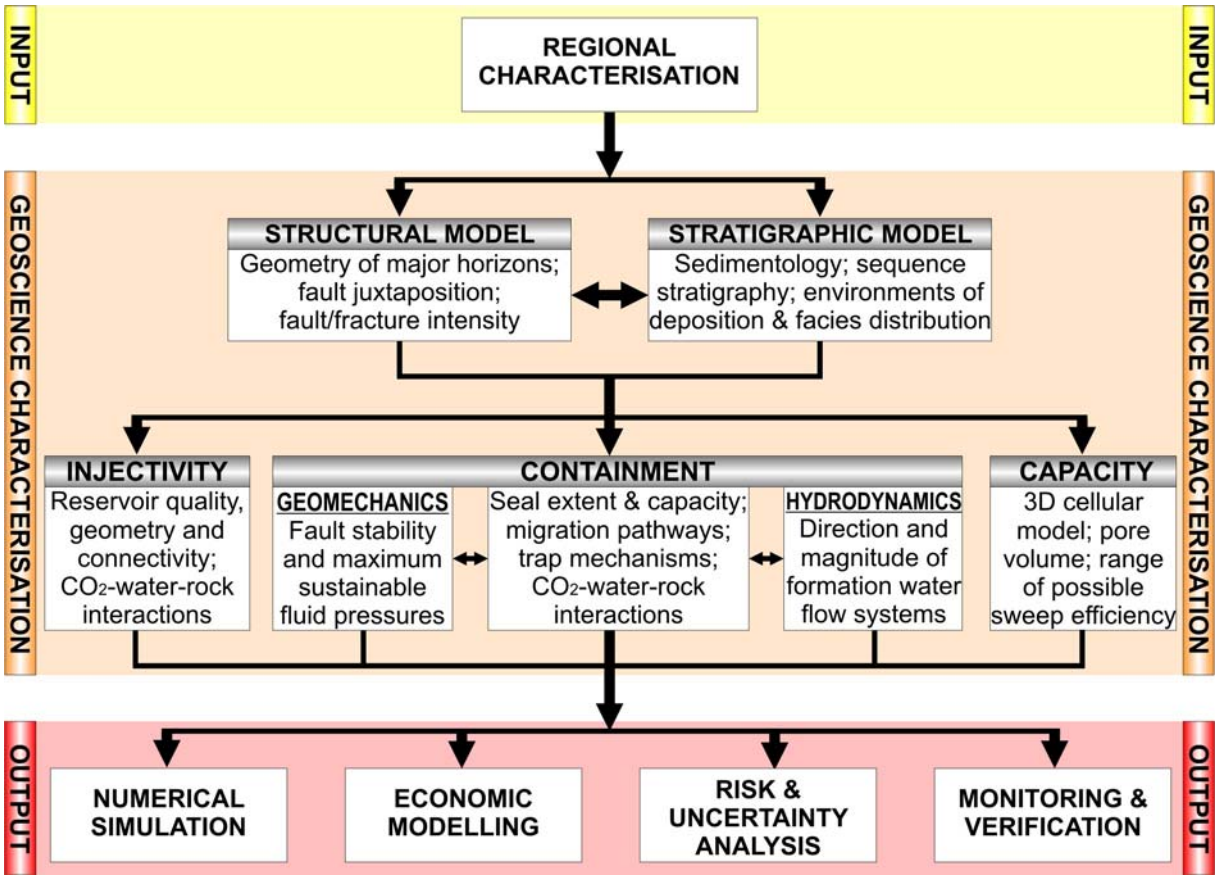

Figure 5.6 Workflow followed to geologically characterise potential sites for geological storage of CO_2.

Factors that influence injectivity include the geometry and connectivity of individual flow units, the nature of the heterogeneity within those units (i.e. the likely distribution and impact of baffles such as interbedded siltstones and shales) and the physical quality of the reservoir in terms of porosity and permeability characteristics (Figure 5.6). The sedimentary depositional models derived from the sequence stratigraphic interpretation provided information about the reservoir distribution and the likely lateral and vertical connectivity, as the geometry and

spatial distribution of individual flow units is a function of their environment of deposition. The reservoir quality was assessed via detailed analysis of core plug porosity and permeability characteristics, petrography and wireline log petrophysical interpretation. The petrographic study was undertaken by Kraishan (2000) and the petrophysics interpretation was provided by Skinner (2000), the key results of which were integrated into this study.

Factors relating to containment include the distribution and continuity of the seal, the seal capacity (maximum CO_2 column height retention), potential migration pathways (structural geometry, distribution and extent of intraformational seals, and formation water flow direction and rate) and the integrity of the reservoir and seal (fault/fracture stability and maximum sustainable pore fluid pressures) (Figure 5.6). Collected core samples were subjected to mercury injection capillary pressure (MICP) analysis to evaluate the CO_2 retention capacity of the rocks. Geomechanical studies by Streit (2001) used *in situ* stress and rock strength data to determine fault reactivation potential, the results of which were integrated into this study to assess the reactivation risk of faults in the area. The past and present formation water flow systems were characterised by Bekele and Otto (2000) from pressure-elevation plots and hydraulic head distribution maps, and integrated into this study to interpret the possible impact on CO_2 migration and containment.

Potential CO_2 storage capacity was assessed geologically in terms of available pore volume; however, the efficiency of that storage capacity will be dependent on the rate of CO_2 migration, the potential for fill-to-spill structural closures encountered along the migration path, and the long-term prospects of residual trapping, dissolution into the formation water or precipitation into new carbonate minerals (Figure 5.6). The pore volume was estimated using the calculation method described in Chapter 3.

5.4 STRUCTURAL MODEL

The structural model defines the gross geometry of the reservoir and seal units and identifies structural features such as faults and salt diapers. The structural framework is critical to understanding and predicting how injected CO_2 will migrate within the subsurface over the long-term. The structural framework of the Petrel Sub-basin was constructed using the seismic interpretation and well correlation.

5.4.1 Structural Geometry

Ten surfaces representing significant stratigraphic horizons were interpreted on the

seismic data across the Petrel Sub-basin. The interpreted horizons are distinctive seismic events that can be correlated across the study area and which define discrete stratal packages of similar seismic character. Details of the interpreted surfaces are listed in Table 5.1 and Figure 5.7 shows the relationship of the interpreted surfaces to an intersecting well in the centre of the basin. Figure 5.8 shows the seismic interpretation along a regional strike line (100/03) and regional dip line (100/05), highlighting the gross structural geometry across the basin, and Figure 5.9 shows a more detailed view of the seismic character and interpretation over the Petrel Field area.

Table 5.1 Details of interpreted seismic surfaces.

Seismic Surface	**Lateral Extent**	**Key Stratal Relationships**
Near Top Bathurst Island Gp †	Across whole of area of interest	Toplap surface for underlying strata
Top Sandpiper Sst/Base Bathurst	Across whole of area of interest	Downlap surface for overlying strata
Intra-Sandpiper Sst	Absent in south	Toplap surface for underlying strata
Top Frigate Fm/Base Sandpiper Sst	Basin centre only	Downlap surface for overlying strata
Intra-Frigate Fm (2)	Absent in north	Onlap surface for overlying strata
Intra-Frigate Fm (1)	Central and southern area only	Downlap surface for overlying strata
Top Elang Fm/Base Frigate Fm	Across whole of area of interest	Onlap surface for overlying strata
Top Plover Fm/Base Elang Fm	Across whole of area of interest	Downlap surface for overlying strata
Intra-Plover Fm	Partially absent S and SE margins	Truncates underlying strata
Base Plover Fm	Across whole of area of interest	Truncates underlying strata

† The Bathurst Island Group extends to the Cretaceous/Tertiary boundary; however, it was thought somewhat unrealistic to treat the entire succession as regional seal, as vertically it becomes siltier and sandier towards the top. Therefore, the Near Top Bathurst surface was picked at a prominent reflector within the succession below the Cretaceous/Tertiary boundary.

Depth converted structural surfaces of the key reservoir and seal bounding horizons mapped from the seismic interpretation are shown in Figure 5.10, Figure 5.11, Figure 5.12 and Figure 5.13. The structural geometry of all the horizons is very similar. All the surfaces are shallowest around the southwest, south and southeast margins of the basin and deepen into the basin centre and to the northwest. From these depth surfaces, it can be seen that the Mesozoic succession within the Petrel Sub-basin is structurally simple, reflecting the gentle sag deposition of the post-rift sediments. The strata dip gently up towards the southwest, south and southeast from their deepest point in the northwest and onlap onto the flanking shelves of Proterozoic basement. A weakly developed, unclosed anticlinal structure trends

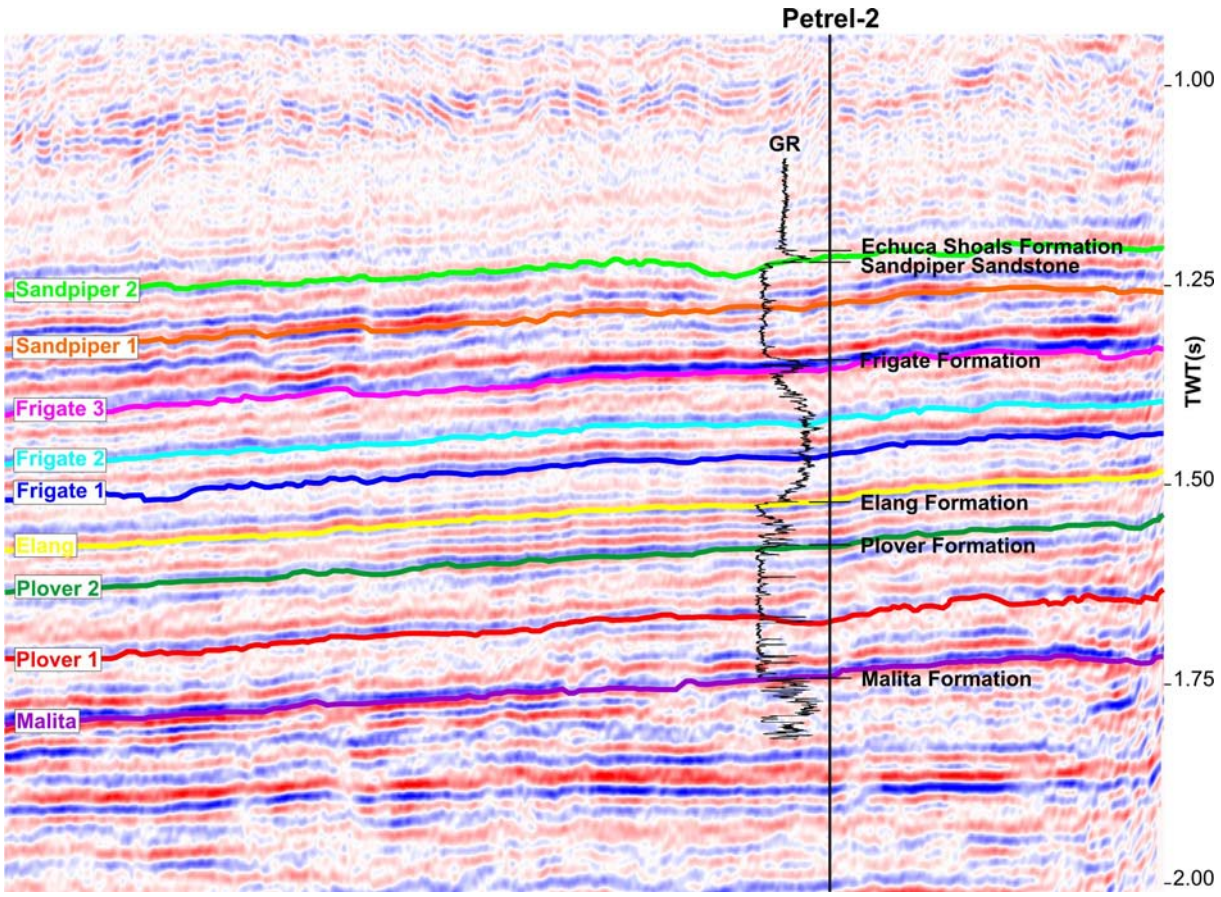

Figure 5.7 Seismic interpretation and tie to Petrel-2 well intersection (seismic line 90bg-124).

along the basin axis in a northwest-southeast direction, reflecting the deeper structural doming in the centre of the basin within the underlying Palaeozoic succession. Despite this slight doming in the centre of the basin, there is no structural closure at the Mesozoic level. Small bullseye features located at Gull-1, Curlew-1, Sandpiper-1 and adjacent to the Tern field are the result of underlying salt diapirs at these locations.

The continuous shallowing of the Mesozoic succession towards the basin margins means that the limit for the phase-change for supercritical CO_2 occurs within the reservoir intervals for both the Plover and Sandpiper ESSCIs. The average pressure and temperature gradients of the Petrel Sub-basin established that the depth for supercritical CO_2 would be reached at about 750 m. Figure 5.14 shows the position of the 750 m depth contour at the Top Elang Formation and Top Sandpiper Sandstone depth structure maps. Within the Plover/Elang reservoir, migrating CO_2 would remain supercritical until about 90 km southeast of the Petrel Field (~20 km northwest of the Bougainville-1 well), whereas for the Sandpiper Sandstone reservoir, this would occur about 70 km southeast of the Petrel Field (~40 km northwest of the Bougainville-1 well).

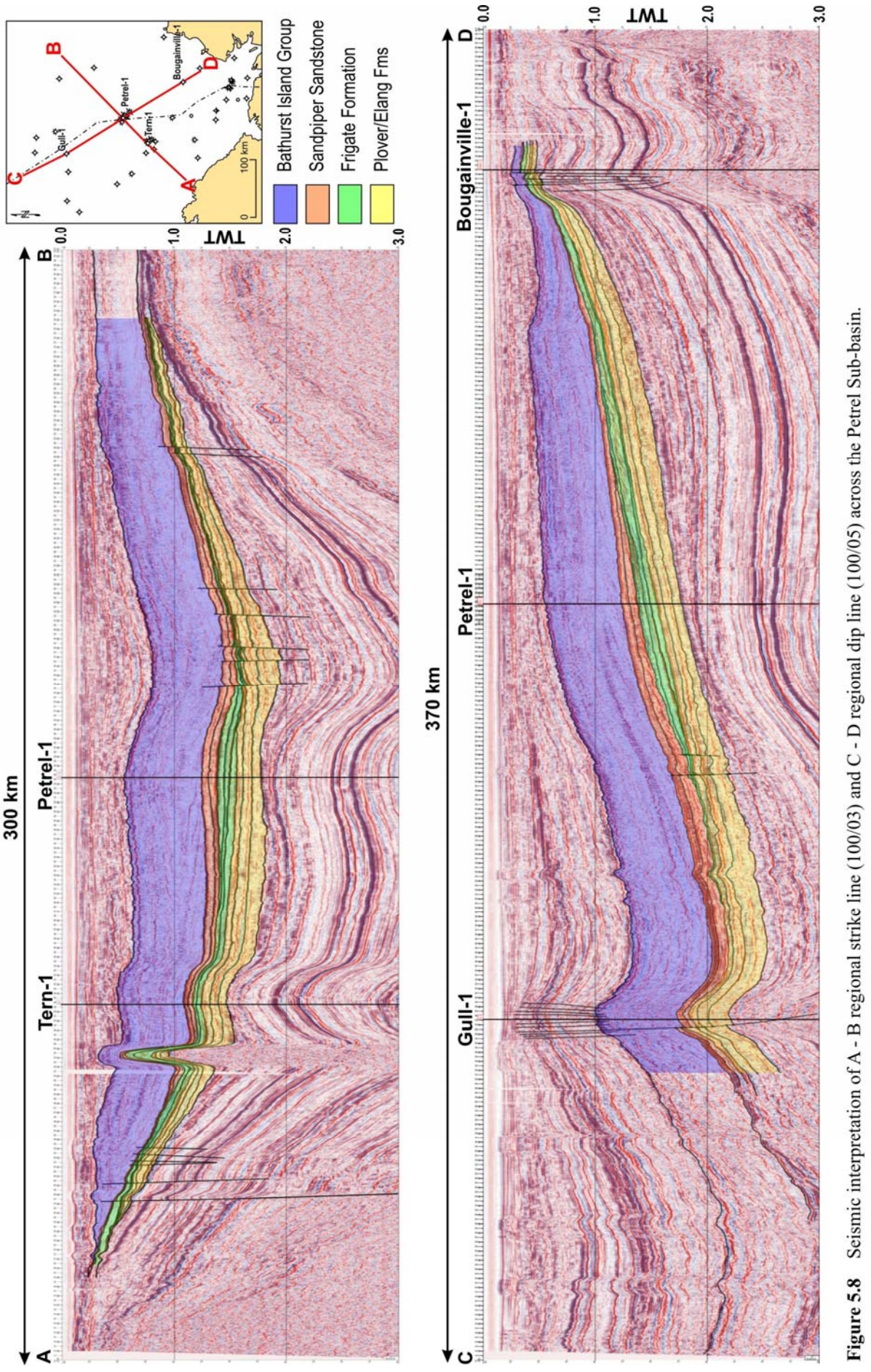

Figure 5.8 Seismic interpretation of A - B regional strike line (100/03) and C - D regional dip line (100/05) across the Petrel Sub-basin.

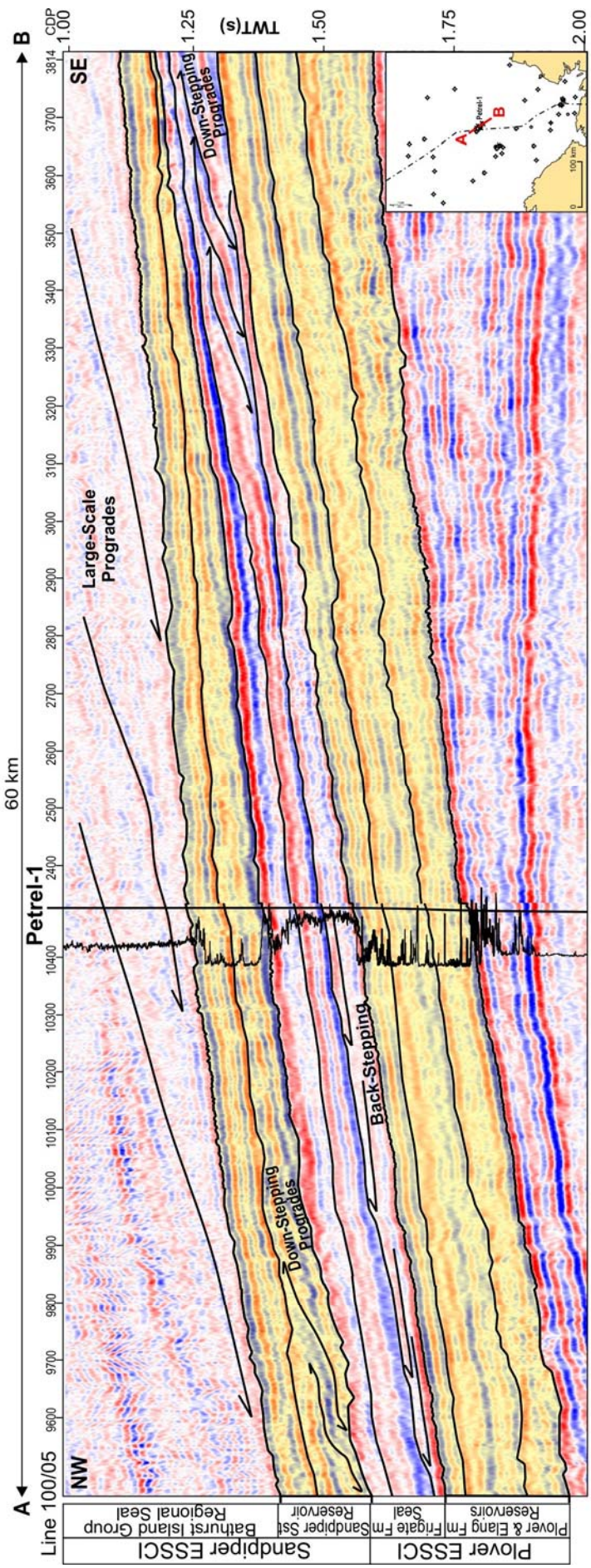

Figure 5.9 Detailed view of the seismic interpretation over part of the regional dip line 100/05 over the Petrel Field area.

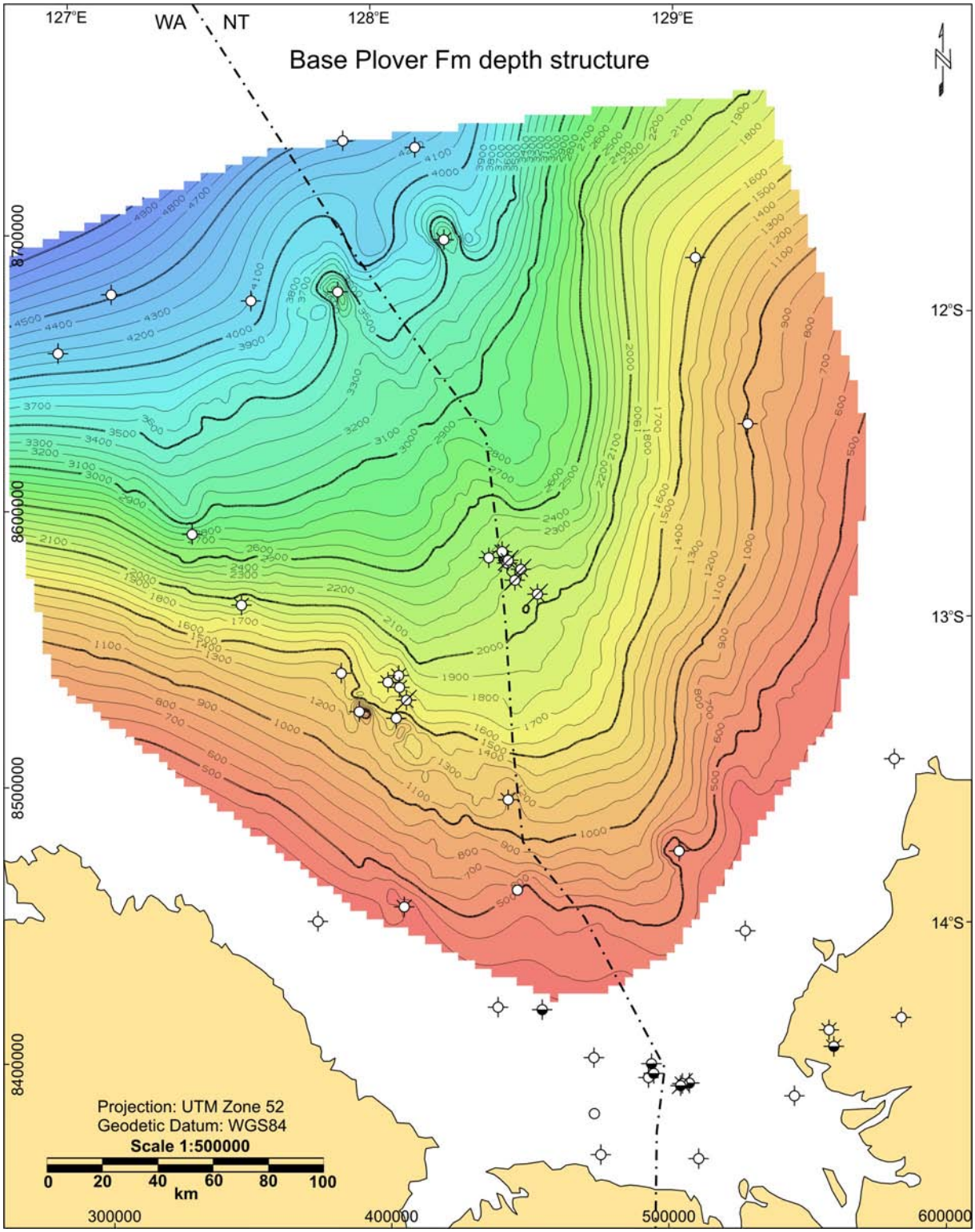

Figure 5.10 Depth structure map of Base Plover Formation seismic surface.

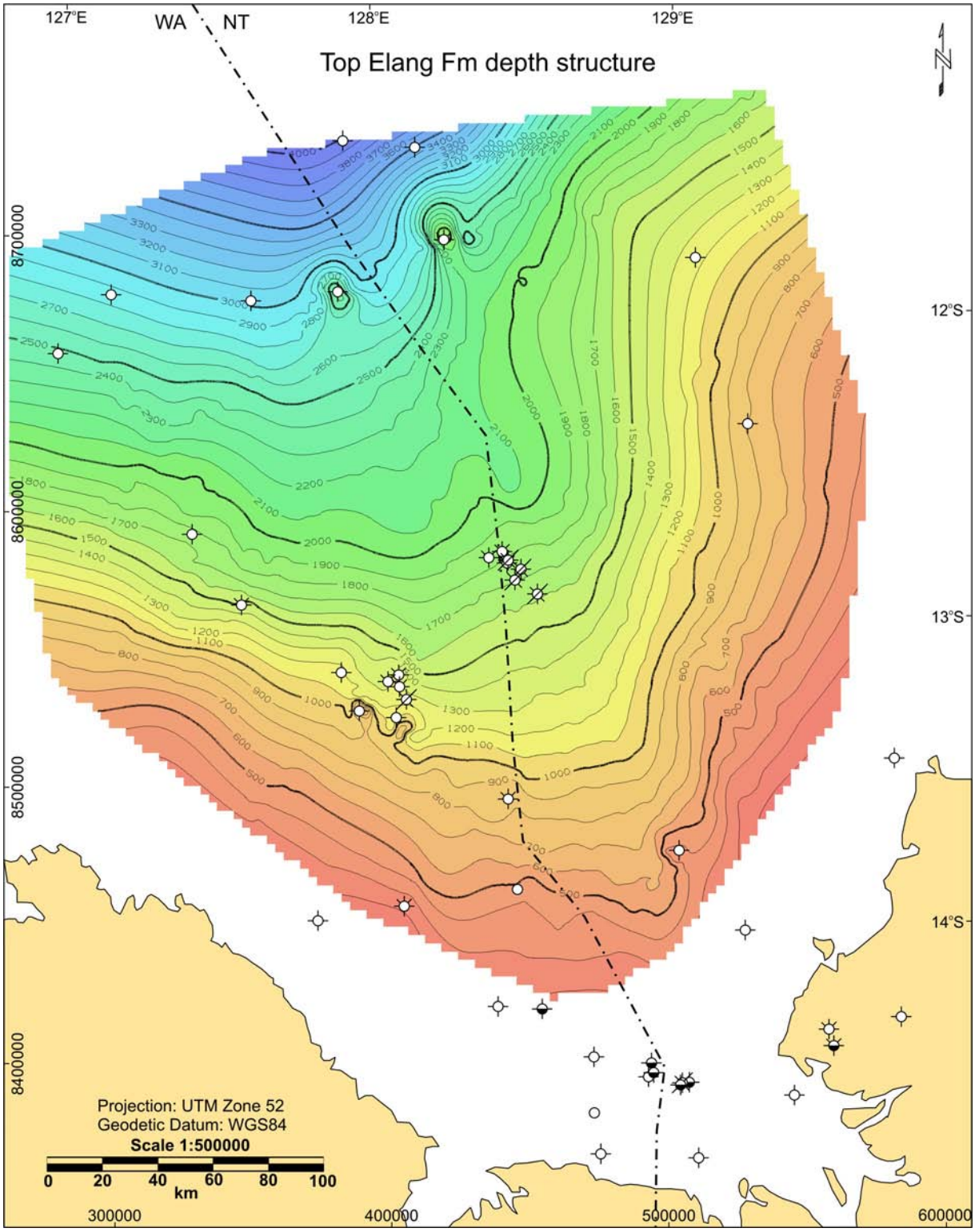

Figure 5.11 Depth structure map of Top Elang Formation seismic surface.

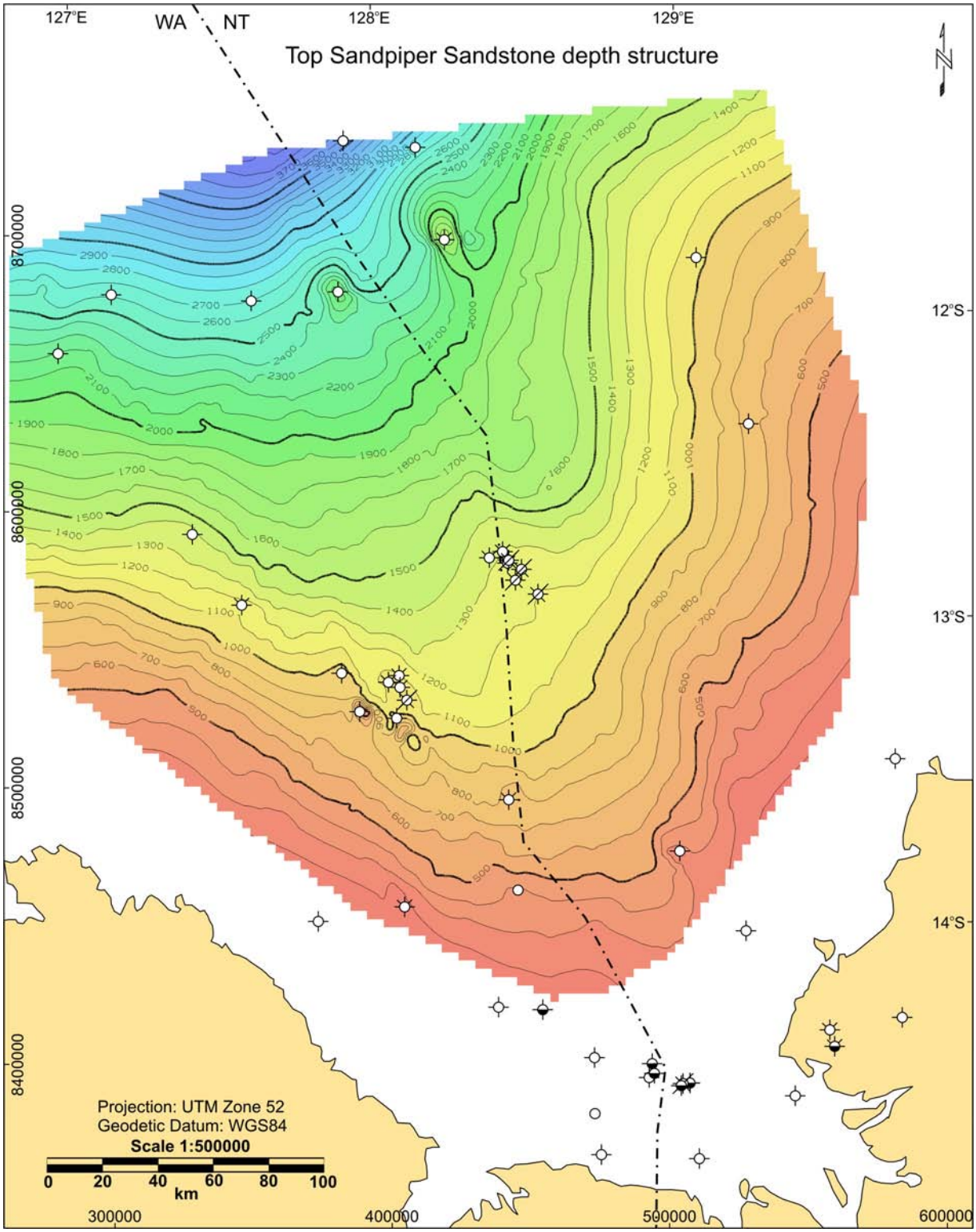

Figure 5.12 Depth structure map of Top Sandpiper Sandstone seismic surface.

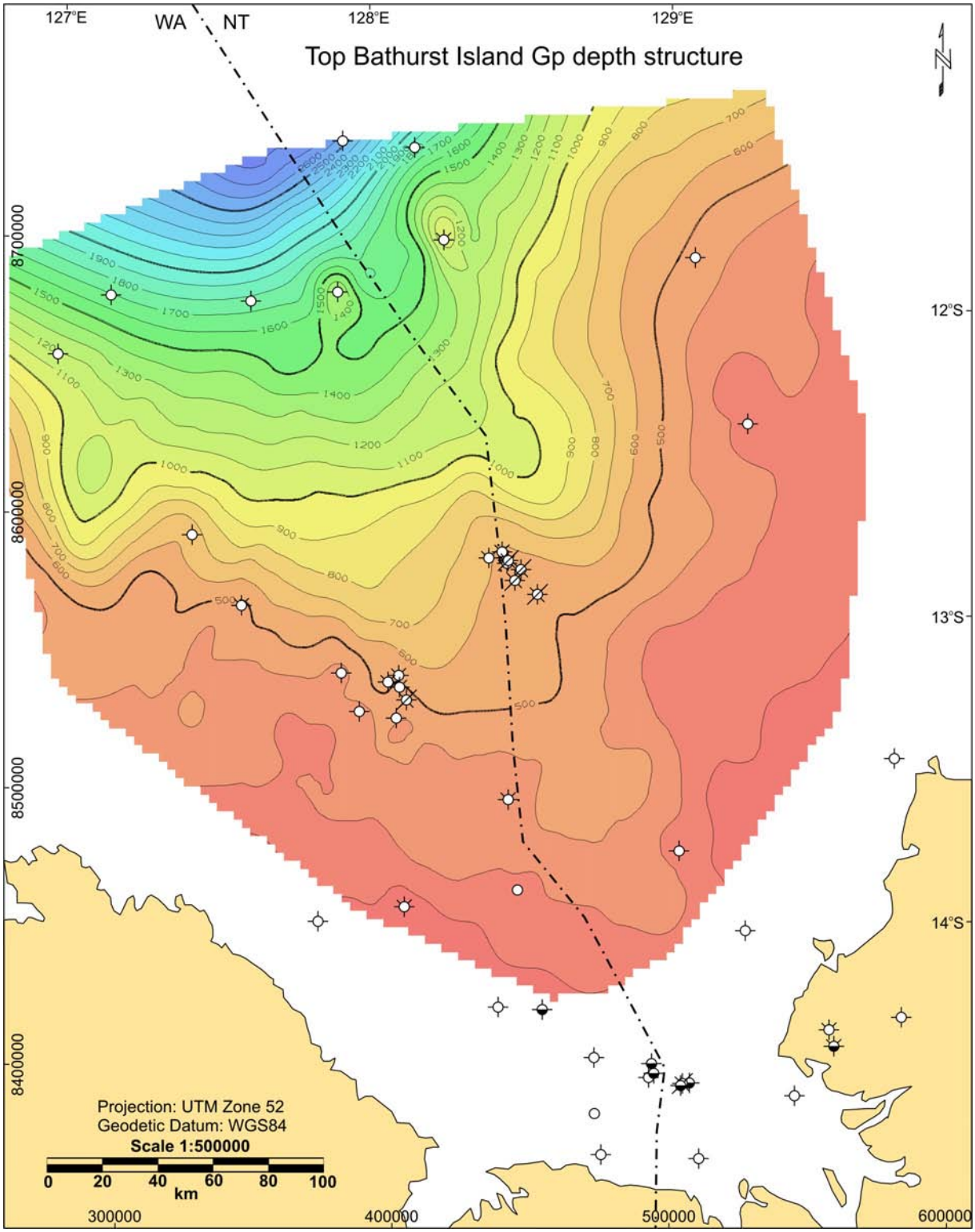

Figure 5.13 Depth structure map of Near Top Bathurst Island Group seismic surface.

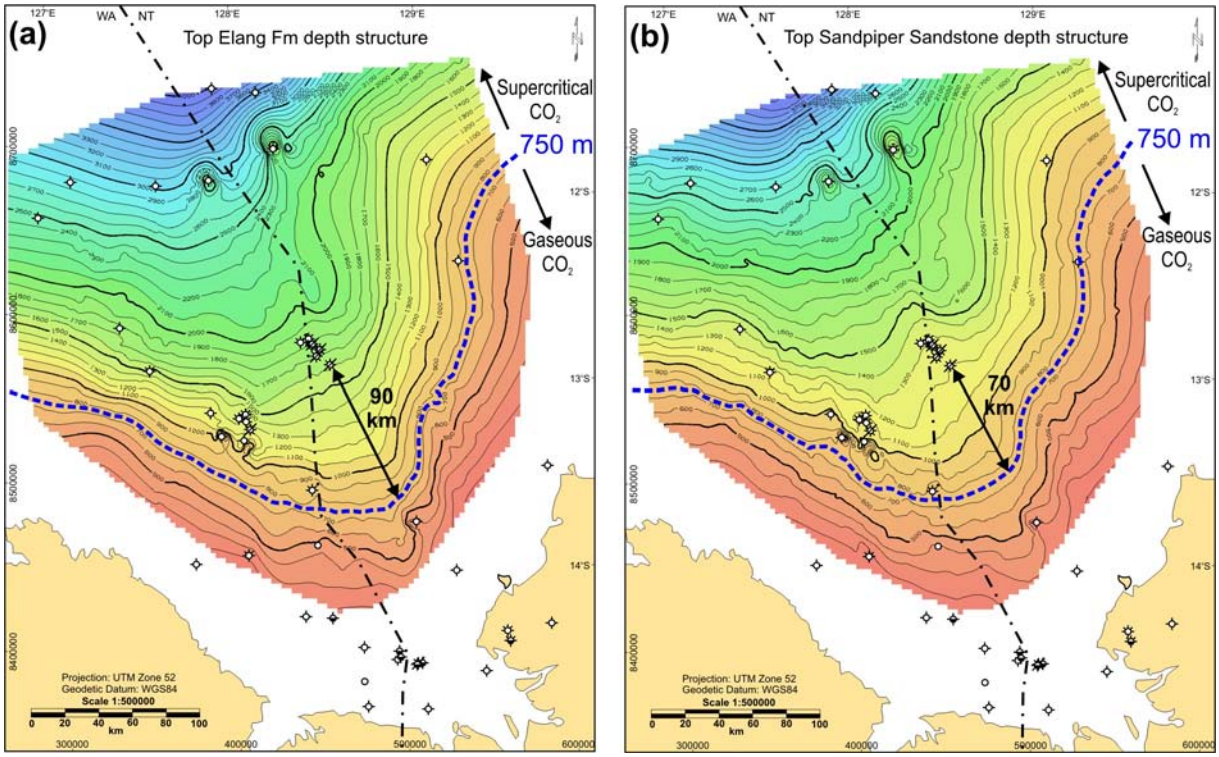

Figure 5.14 Location of 750 m depth contour which represents the limit at which CO_2 will remain in a dense supercritical phase, for: (a) Top Elang Formation (top reservoir/base seal of the Plover ESSCI); and (b) Top Sandpiper Sandstone (top reservoir/base seal of the Sandpiper ESSCI).

5.4.2 Fault Characteristics

The post-rift sediments in the Petrel Sub-basin are relatively unfaulted. The major faults that are found in the Petrel Sub-basin generally occur around the basin margins (Figure 5.3 and Figure 5.15a). They strike in a northwest direction and dip at angles of 60–70º, connecting to basement detachment zones at mid-crustal depths (O'Brien *et al.*, 1993; O'Brien *et al.*, 1996). Other large-scale faults sometimes occur in association with salt diapers; for example, the fault located alongside the diapir beneath Curlew-1 (Figure 5.15b). Minor faulting observed within the Mesozoic succession includes a small graben feature to the northeast of the Petrel Field, which can be seen on seismic line 100/03, penetrating the reservoir units and but only extending a short way into the overlying regional seal (Figure 5.15c). Unfortunately, modelling of the lateral extent of these faults was not possible due to a lack of seismic data density at this location. Thus, the orientation of these faults (i.e. true dip and strike direction) cannot be determined from the available data.

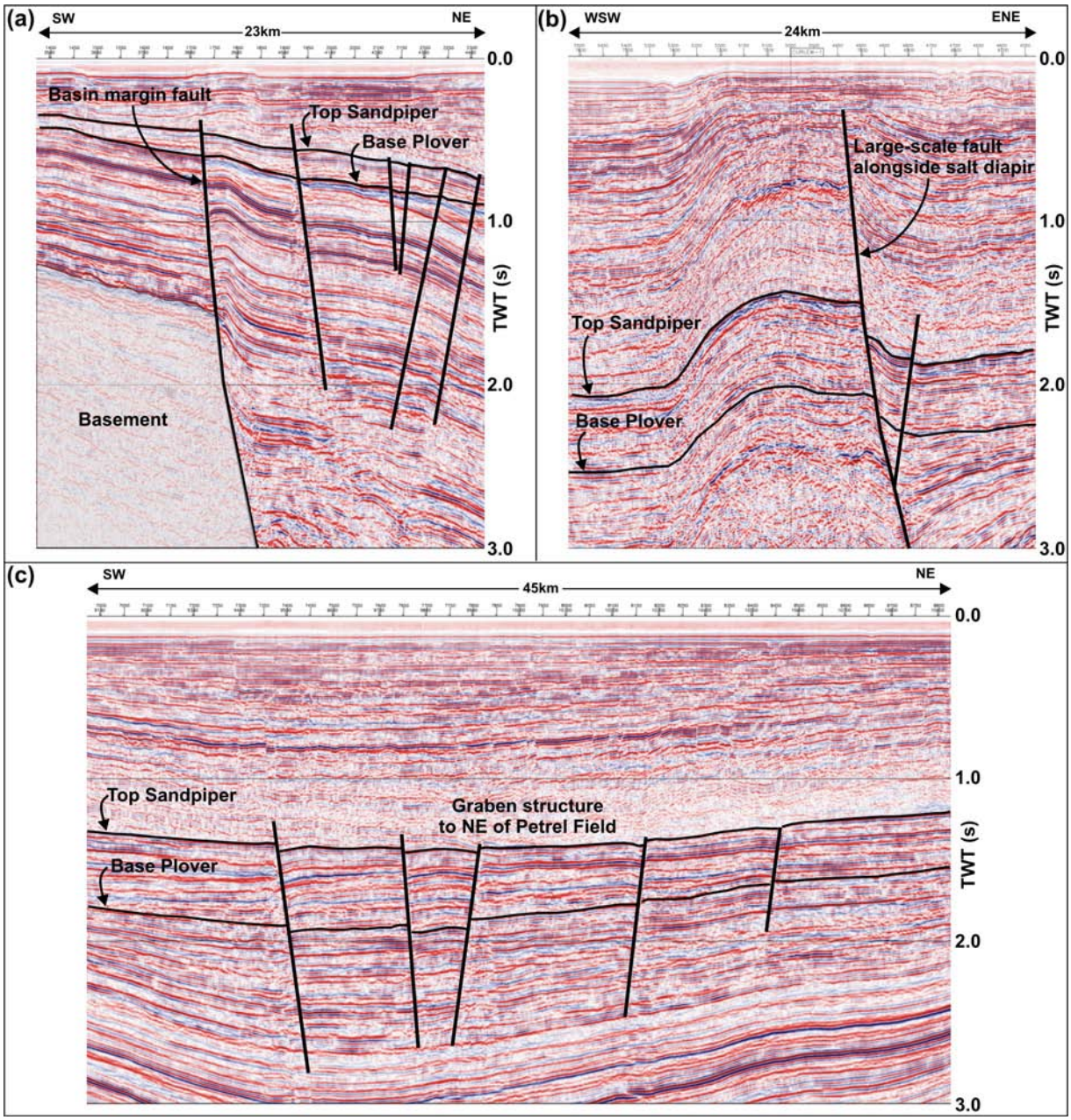

Figure 5.15 Examples of faults identified Petrel Sub-basin. (a) Basin margin fault to the southwest of Sandpiper-1 (seismic line 100/03). (b) Large-scale fault alongside salt diapir at Curlew-1 (seismic line 100/04). (c) Graben structure to the northeast of the Petrel Field (seismic line 100/03).

Small-scale faults are also seen on the seismic sections, distorting bright seismic reflectors at the picked top of the Bathurst Island Group regional seal (Figure 5.16a). These small-scale faults are not seen to extend down through the seal. The brighter seismic reflections that show evidence for faulting are interpreted to be more competent layers within the Bathurst Island Group, such as limestone bands, and thus to deform in a brittle manner. The bulk of the Bathurst Island Group succession comprises mainly mudstones and shales, which are inferred to behave in a more ductile manner, thus the faults don't penetrate through the entire

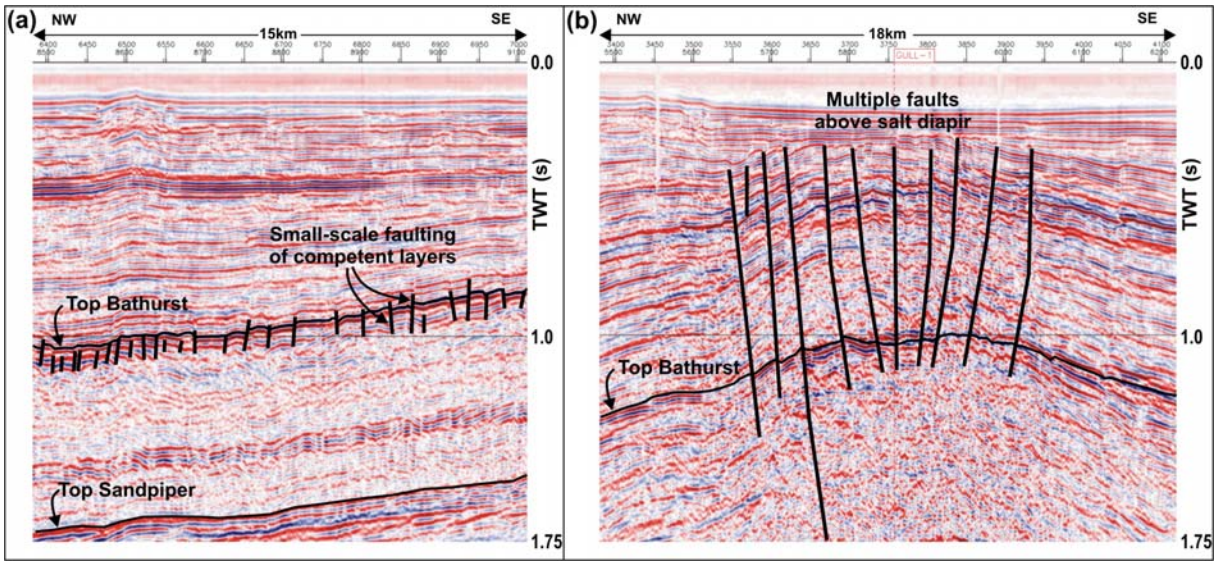

Figure 5.16 Examples of faults identified Petrel Sub-basin. (a) Small-scale faulting within competent layers of the Bathurst Island Group regional seal (seismic line 100/05a, northwest of Petrel-1). (b) Dense collection of faults above the salt diapir at Gull-1 (seismic line 100/05a).

section, but are apparently contained within it. Another type of faulting identified in the Petrel Sub-basin is dense collections of smaller-scale faulting occurring in the strata immediately above salt diapers. An example of this is seen at Gull-1 (Figure 5.16b). The resolution of the seismic data is poor in the vicinity of the salt diapers, so it is difficult to determine the likely interconnectivity of these faults.

On the whole, faulting in the Petrel Sub-basin within the interval of interest is relatively minor. The faults that may pose a risk to containment occur predominantly around the basin margins, generally outside the likely CO_2 storage area, or in conjunction with known salt diapirs, which are not likely to be within the primary CO_2 migration pathway. The geomechanical stability of the faults is addressed later in section 5.7.4.

5.5 STRATIGRAPHIC MODEL

The stratigraphic model determines the sedimentary environments of deposition and likely facies distribution, both laterally and vertically. The stratigraphic framework is important for understanding the distribution of reservoir properties (such as porosity and permeability), which are critical for the ease with which CO_2 can be injected, how it might disperse and the volume that can be stored. The stratigraphy of the Petrel Sub-basin was evaluated through the sedimentology, well correlation, seismic facies and sequence stratigraphic interpretation.

5.5.1 Sedimentology

The sedimentological data available over the interval of interest within the Petrel Sub-basin was rather sparse, due to the Mesozoic succession not being the hydrocarbon-producing interval. However, some sedimentary core was available from the Petrel-1 and Gull-1 wells. A total of 19 lithofacies were identified from within the cored intervals, based on variations in characteristics such as colour, bedding, composition, texture, fossils and sedimentary structures. Examples of the various lithofacies are shown in Figure 5.17 and described in Table 5.2. The lithofacies were grouped together into facies associations and an interpretation made as to their possible depositional environment. Six facies associations were identified in total and are described below (Table 5.2).

5.5.1.1 Facies Association A – Braided Fluvial Channels

Facies Association A comprises lithofacies 1 to 4, and is representative of the Plover Formation. The relatively coarse grain size and the lack of mud matrix material suggest that the rocks were deposited within a high energy, bedload-dominated environment. The presence of cross-bedding identified in some of the beds implies traction currents and channelised flow. The presence of coaly fragments and lack of marine fossils within the sandstones indicates that the rocks were likely to have been deposited within a non-marine environment. Therefore, the probable environment of deposition was within non-marine fluvial channels. A braided fluvial system is interpreted because of the high sandstone/shale ratio; however, they could also include amalgamated meandering stream deposits, especially near the top of the Plover Formation. Some of the coal is likely to have developed from either wood or branches, or as peat in the vicinity of the area that was eroded into by new channels. The rapidly fining-up units with the very coarse and granule-sized material at the base could be the result of the initiation and abandonment of new channels. The thin siltstone units were probably deposited in overbank environments or possibly at abandoned channel fill. However, the general lack of fine-grained sediments suggests that the overbank environment had a low preservation potential, and that the mobile braided channels formed a laterally extensive complex of channelised sand bodies, with very little chance for preservation of fine-grained overbank sediments.

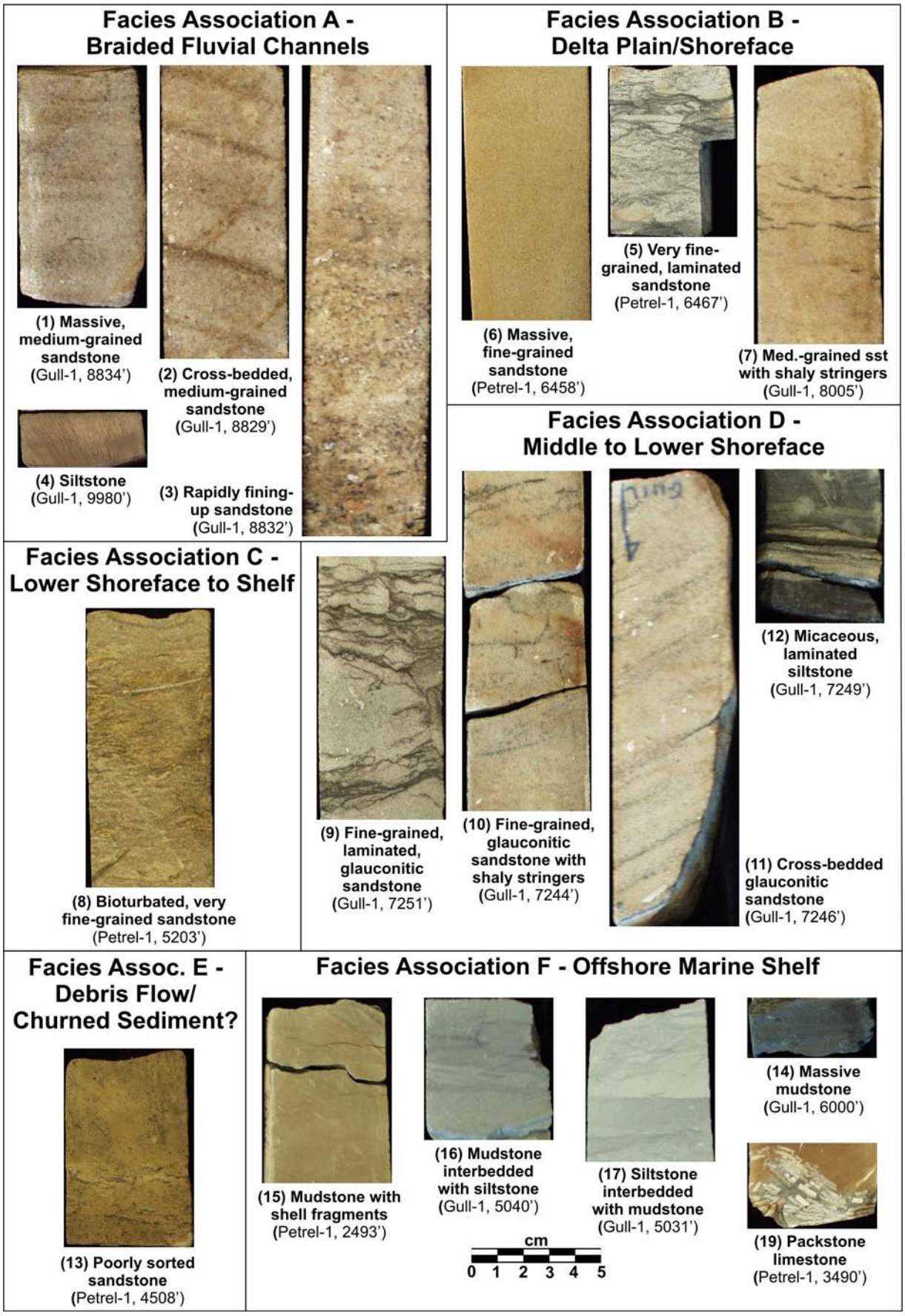

Figure 5.17 Core photographs of lithofacies and their interpreted facies associations.

Table 5.2 Sedimentary core lithofacies, facies associations and interpreted depositional environments.

Fm	No	Name	Lithofacies Description	Facies Association – Interpretation	
BATHURST ISLAND GROUP	19	Packstone limestone	Grey to brown, grain supported limestone composed of shell fragments and micrite matrix.	FACIES ASSOCAITION F	Offshore marine shelf
	18	Micritic limestone	Grey, micritic limestone.		
	17	Siltstone interbedded with mudstone	Hard, blocky, greenish siltstone interbedded with dark greenish-grey mud laminae.		
	16	Mudstone interbedded with siltstone	Dark greenish-grey, massive mudstone with a hard, blocky texture. Mudstone is thinly interbedded with greenish siltstone.		
	15	Mudstone with shell fragments	Dark grey to greenish-grey, massive mudstone with a hard, blocky texture; often contains shell fragments.		
	14	Massive mudstone	Dark grey to greenish-grey, massive mudstone with a hard, blocky texture that occasionally displays some fissility.		
SANDPIPER SANDSTONE	13	Poorly sorted sandstone	Light grey, poorly consolidated (friable), compositionally mature sandstone. Mean grain size is fine sand, however, grains of medium to very coarse sand and occasional granule-sized grains also exist. Grain texture ranges from sub-angular to sub-rounded. Wavy mud laminations sometimes exist.	FACIES ASSOC. E	Debris flow/ churned sediment?
	12	Micaceous, laminated siltstone	Quartz-rich siltstone with a moderate amount of mica. Fine-grained sandstone laminae and minor bioturbation is resolvable.	FACIES ASSOCIATION D	Middle to lower shoreface
	11	Cross-bedded, glauconitic sandstone	Cross-bedded, compositionally mature sandstone with minor amounts of glauconite. Sandstone is fine-grained, well sorted, with sub-angular to sub-rounded grains. Glauconitic grains are preferentially aligned along cross-bed foresets.		
	10	Fine-grained, glauconitic sandstone with flaser bedding	Fine-grained sandstone with minor amounts of glauconite. Sandstone is compositionally mature, well sorted, with sub-angular to sub-rounded grains. With the exception of occasional flaser bedding, the sandstone is massive, with little resolvable structure.		

Fm	No	Name	Lithofacies Description	Facies Association – Interpretation	
SANDPIPER	9	Fine-grained, laminated, glauconitic sandstone	Fine-grained sandstone with minor amounts of glauconite. Sandstone is compositionally mature, well sorted, with sub-angular to sub-rounded grains. Wavy and flat/parallel mud laminations and vertical burrow traces are present.	FACIES ASS. D	Middle to lower shoreface
FRIGATE FM	8	Bioturbated, very fine-grained sandstone	Bioturbated, very fine-grained, moderately sorted, silty sandstone. Bioturbation over-prints primary structure; however, thinly interbedded layers of very fine-grained sandstone and siltstone are resolvable. Burrows are sub-horizontal to inclined. Shell fragments and calcareous nodules are often present.	FACIES ASSOC. C	Lower shoreface to shelf
ELANG FM	7	Medium-grained, sandstone with shaly stringers	Massive (structureless), medium-grained sandstone, compositionally and texturally mature, with sub-angular to sub-rounded grains. Sandstone is often associated with flaser bedding(?), stylolites, coaly stringers, occasional siltstone rip-up clasts, pyrite nodules and minor bioturbation.	FACIES ASSOCIATION B	Delta plain/ shoreface
PLOVER FM	6	Massive, fine-grained sandstone	Massive (structureless), fine-grained and well sorted sandstone. Sandstone is compositionally and texturally mature. Framework grains are sub-angular to well rounded. Occasional mud laminae and stylolites are present.		
	5	Very fine-grained, laminated sandstone	Laminated fine-grained sandstone with sub-angular and sub-rounded grains. Compositionally mature with a small amount of mud matrix. Occasional stylolites and mud laminae are present.		
	4	Siltstone	Grey siltstone, with a hard, blocky texture.	FACIES ASSOCAITION A	Braided fluvial channels
	3	Fining upward (graded), sandstone and conglomerate	Wavy laminated, well sorted sandstone with occasional cross-bedding (in upper sections). Grain size varies from granule-sized gravel to medium-grained sand up-section (coarse-tail, normal grading). Framework grains are dominantly quartz with a small amount of mud matrix.		
	2	Cross-bedded, medium-grained sandstone	Cross-bedded, fine- to medium-grained sandstone. Compositionally mature, clast supported, with sub-rounded to rounded grains and minor pyrite nodules.		

Fm	No	Name	Lithofacies Description	Facies Association – Interpretation	
PLOVER FM	1	Massive medium- to coarse-grained sandstone	Massive (structureless), medium- to coarse-grained sandstone. Compositionally mature, clast supported with sub-rounded to rounded grains. Frequently associated with stylolites, coaly stringers and pyrite nodules.	FACIES A	Braided fluvial channels

5.5.1.2 Facies Association B – Delta Plain/Shoreface

Facies Association B comprises lithofacies 5 to 7, and is representative of the top of the Plover Formation and the Elang Formation. The sand-sized sediment with very little matrix suggests a moderate to high energy depositional environment, whereas the very fine-grained sandstones with mud lamination suggest a slightly lower energy depositional environment. The presence of coaly fragments within the sandstones indicates that fossil wood and branches were transported within the sediment, but the minor amounts of glauconite (e.g. lithofacies 6) suggest a shallow marine influence. These rocks, therefore, are interpreted as delta plain, where both fluvial and marine processes can influence the sedimentation. The sand-sized sediment is most likely to have been deposited within distributary fluvial channels or reworked into a shoreface deposit. The finer grained sandstone with mud laminae and bioturbation are perhaps more indicative of interdistributary bays.

5.5.1.3 Facies Association C – Lower Shoreface to Offshore Marine Shelf

Facies Association C comprises lithofacies 8, and is representative of the Frigate Formation. The fine grain size indicates a fairly low energy depositional environment and the intensity of the bioturbation suggests that the rate of sedimentation was quite slow. The presence of shell fragments indicate that the rocks were deposited within a marine environment. The sub-horizontal or inclined orientation of the burrow traces are possibly representative of the *Cruziana* ichnofacies type. The environment of deposition is therefore likely to be on a shallow marine shelf, in the lower shoreface to offshore region.

5.5.1.4 Facies Association D – Middle to Lower Shoreface

Facies Association D comprises lithofacies 9 to 12, and is representative of the Sandpiper Sandstone. The sandstone is interspersed with mudstone laminae and thin siltstone beds, suggestive of fluctuating energy levels. In Gull-1 core 4 (Appendix F), bioturbated sandstone

is overlain by increasingly clean sandstone, suggestive of an upwardly-shoaling succession. The presence of cross-bedding identified in some of the beds implies traction currents, but the presence of glauconite within the sandstones indicates that the rocks were likely to have been deposited within a shallow marine environment. The vertical orientation of the burrow traces are possibly representative of the *Skolithos* ichnofacies type. The environment of deposition is interpreted as shallow marine, most probably from middle to lower shoreface region. It is most likely these represented linear shorelines striking in a crescent shape across the Petrel Sub-basin, representing infilling from both the southwest and southeast.

5.5.1.5 Facies Association E – Debris Flow/Churned Sediment?

Facies Association E comprises lithofacies 13, and occurs only in the Sandpiper Sandstone, of which there is only a small sample in the core (Petrel-1 core 3; Appendix F). The poorly sorted nature of the rock and the moderate abundance of mud matrix indicates that the sediment was deposited perhaps as a debris flow. Alternatively, it may represent a churned sediment by intensive bioturbation, mixing coarse and fine grained sediment.

5.5.1.6 Facies Association F – Offshore Marine Shelf

Facies Association F comprises lithofacies 14 to 19, and it is representative of the Bathurst Island Group. The mud and silt grain sizes indicate a low energy depositional environment, away from the influence of any currents. The presence of shell fragments and thin limestone beds suggests that the rocks were deposited within a marine environment. Therefore, the probable environment of deposition was on the offshore marine shelf.

5.5.2 Wireline Log Well Correlation

The wells in the Petrel Sub-basin were interpreted in terms of their key stratigraphic surfaces, such as flooding surfaces and sequence boundaries, based on the stacking patterns and wireline log motifs of the gamma ray (GR) and sonic (DT) logs. Key sequence stratigraphic surfaces were interpreted between the *C. torosa* and *P. infusorioides* palynological zones of the Early Jurassic to Late Cretaceous. Figure 5.18 shows an example of the sequence stratigraphic interpretation of Petrel-1. The wells were then correlated across the area using a combination of the biozonation information, the interpreted depositional environments, the seismic stratigraphic packages and stratal relationships, and the wireline log

motifs and key stratigraphic surfaces. Figure 5.19, Figure 5.20 and Figure 5.21 give examples of the regional well correlation.

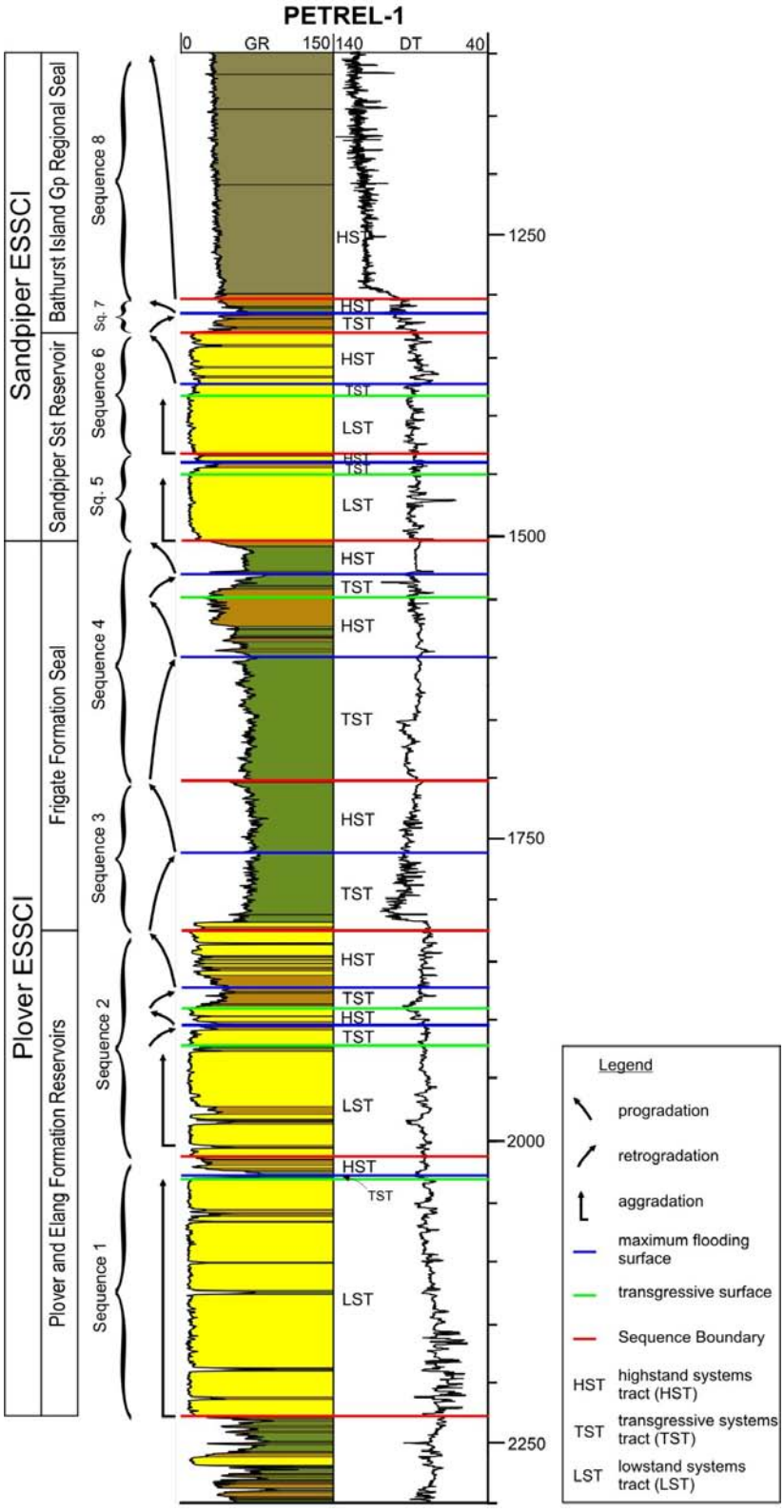

Figure 5.18 Example of the sequence stratigraphic well interpretation of Petrel-1, highlighting the stacking pattern motifs of the gamma ray (GR) wireline log and the interpreted system tracts and sequences.

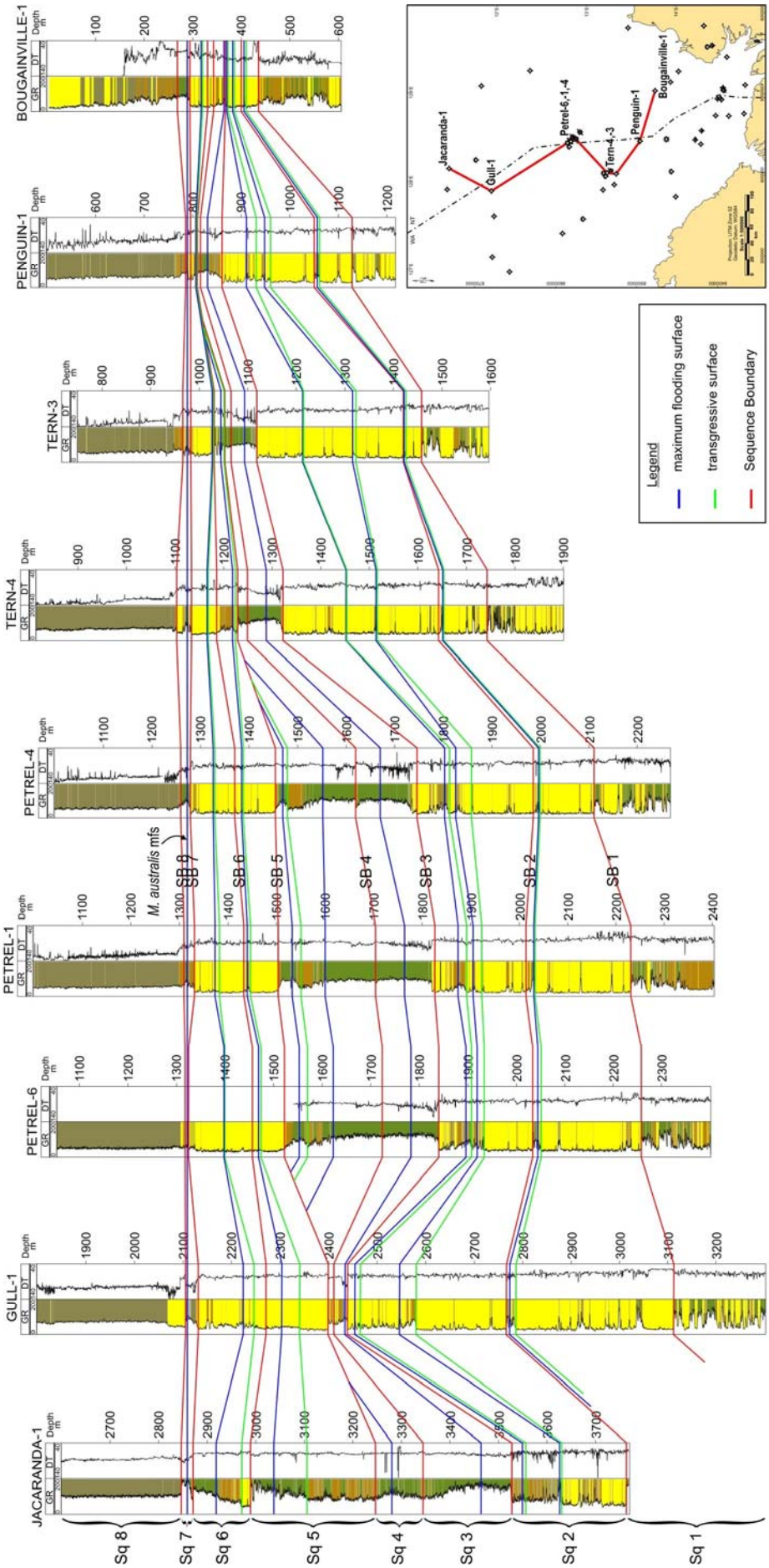

Figure 5.19 Regional well correlation from Jacaranda-1 to Bougainville-1, depicting the sequence stratigraphic interpretation. The correlation is flattened on the *M. australis* maximum flooding surface, near the base of the Bathurst Island Group regional seal.

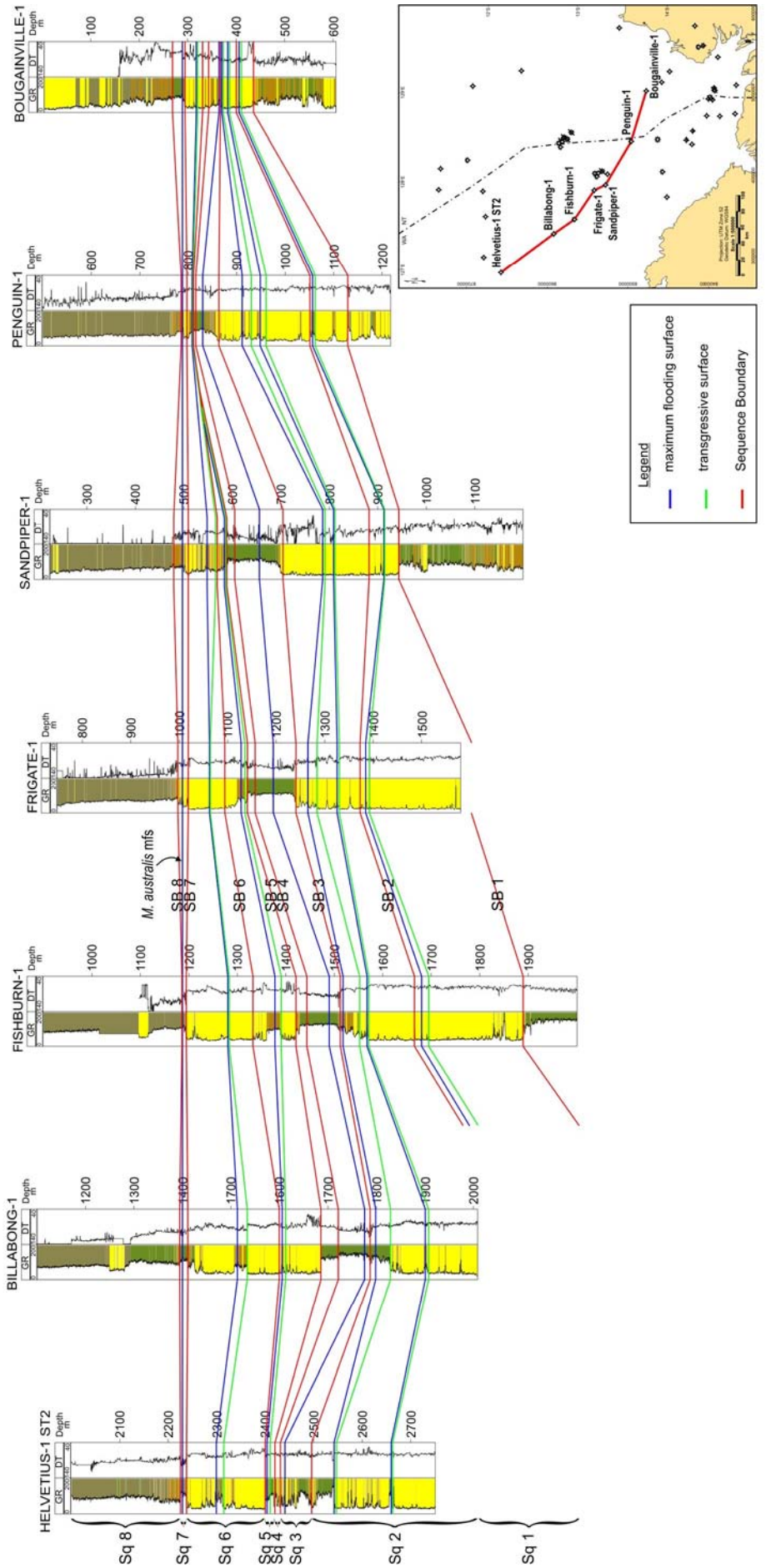

Figure 5.20 Regional well correlation from Helvetius-1 ST2 to Bougainville-1, depicting the sequence stratigraphic interpretation. The correlation is flattened on the *M. australis* maximum flooding surface, near the base of the Bathurst Island Group regional seal.

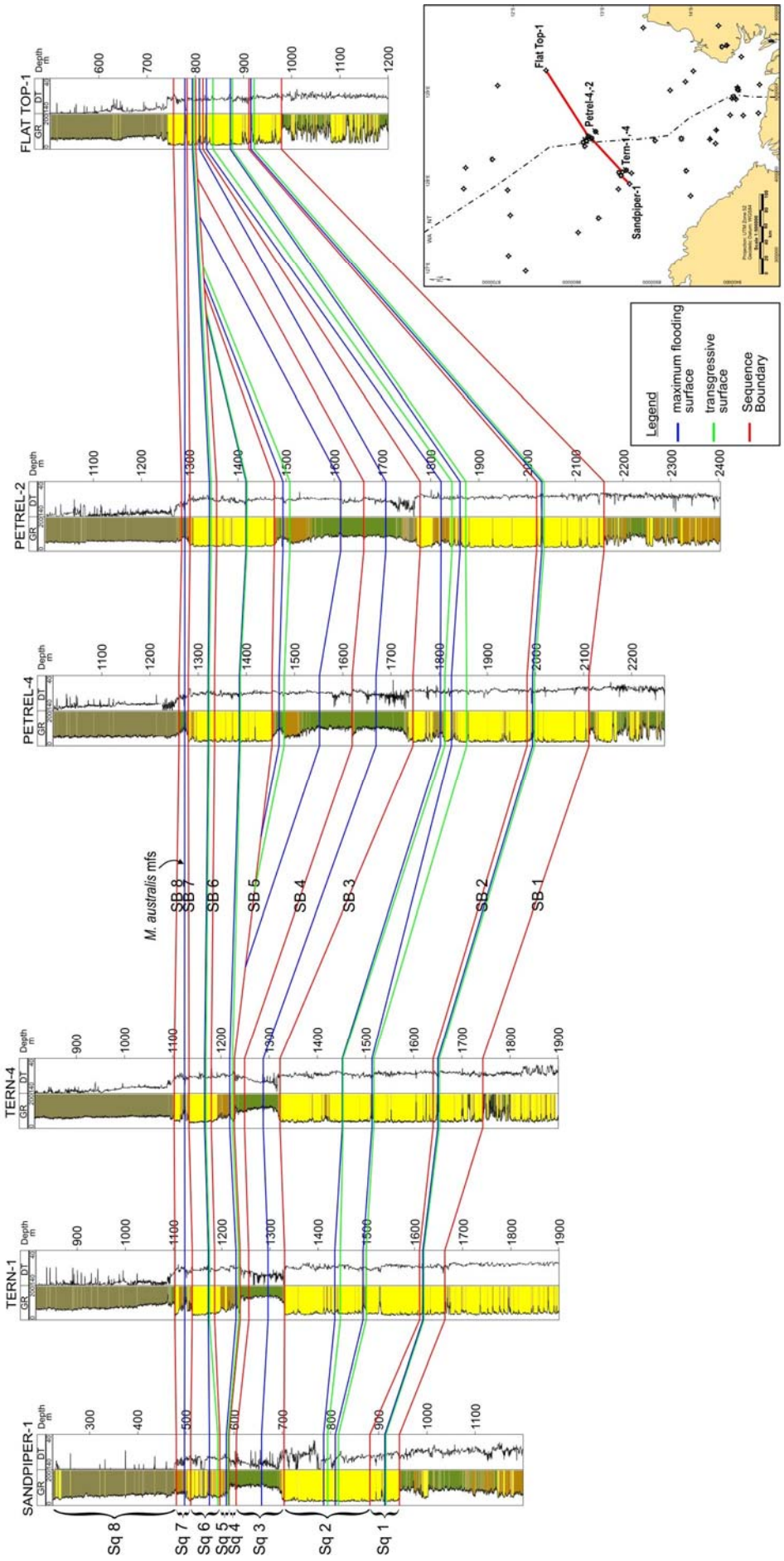

Figure 5.21 Regional well correlation from Sandpiper-1 to Flat Top-1, depicting the sequence stratigraphic interpretation. The correlation is flattened on the *M. australis* maximum flooding surface, near the base of the Bathurst Island Group regional seal.

5.5.3 Sequence Stratigraphy

The integration of seismic structural and stratigraphic interpretations with detailed sedimentological core descriptions, biostratigraphy and wireline log well correlations enabled a sequence stratigraphic framework for the site to be determined. A sequence stratigraphic approach was adopted because it focuses on key surfaces that naturally subdivide the sediment succession into chronostratigraphic units. This is vital to understanding the likely distribution and connectivity of reservoir and seal properties. The approach followed here is that outlined by Posamentier and Allen (1999), where sequences are defined as relatively conformable successions bounded by unconformities or their correlative conformities, and systems tracts are identified by key stratigraphic surfaces and stacking patterns, in both marine and continental settings.

Eight unconformity-bound sequences were identified in the Petrel Sub-basin from the base of the Plover Formation to the Bathurst Island Group. The sequence stratigraphic interpretation presented here is an alternative to that previously proposed by Messant *et al*. (1994). The sequences and their interpretation are described below.

5.5.3.1 Sequence 1

Sequence 1 comprises a thick lowstand systems tract (LST) with a very thin transgressive systems tract (TST) and highstand systems tract (HST). The palynological resolution is very poor over this interval, but it is thought that the sequence spans the *C. torosa* to *D. complex* palynological zones. The sequence is representative of the lower Plover Formation and is present across the majority of the study area. The base of Sequence 1 is identified from the well logs by a distinct change in the gamma ray (GR) wireline log motif, from an alternating high to low GR signature suggestive of mudstones interbedded with thin sandstones, to a sharp-based, blocky, low GR signature. The seismic shows evidence of truncation of the underlying strata (Late Triassic-Early Jurassic Malita Formation). The LST is represented on the well logs by a thick, aggradational, blocky sandstone, overlain by a very thin, retrogradational TST and topped by a thin progradational HST (Figure 5.18–Figure 5.21).

The cored interval in Sequence 1 lies at Gull-1 and was interpreted as stacked braided fluvial channels (Figure 5.17). This is supported by evidence from the palynology of a number of well completion reports, which note that marine microplanktons are absent and the organic assemblage consists of plant material, spores and pollens. The cuttings descriptions from this interval highlight generally medium- to coarse-grained sandstones, with pebbles

reported in Sandpiper-1. The thick LST of Sequence 1 is likely to be a laterally extensive, amalgamated complex of braided fluvial channels, deposited over a widespread area during low accommodation relative to sediment supply (Figure 5.22a). A small rise in relative sea level resulted in a thin shaly unit of the TST, followed by HST progradation as the relative sea level rise reached its maximum and started to fall.

5.5.3.2 Sequence 2

Sequence 2 comprises a LST and two transgressive-regressive cycles of TST and HST. The sequence spans the *C. cooksoniae* to *W. spectabilis* palynological zones. The LST is representative of the upper Plover Formation and the TST and HST cycles are representative of the Elang Formation. The sequence extends across the whole area of interest in the Petrel Sub-basin. The base of Sequence 2 is identified on the well logs by a sharp return to the blocky, low GR wireline log motif. The seismic shows evidence of truncation of the underlying lower Plover Formation. The LST is represented on the well logs by a thick, aggradational, blocky sandstone, over which lies a retrogradational TST and progradational HST. The retrogradational-progradational stacking pattern is repeated for the 2nd cycle of TST-HST. The TST and HST system tracts are identified on the seismic as gently downlapping reflectors (Figure 5.9, Figure 5.18–Figure 5.21).

The LST is very similar to the LST of Sequence 1, with a blocky GR log motif, terrestrial organic microfossils and dominantly medium- to coarse-grained sandstones identified in the cored intervals and cuttings descriptions (Figure 5.17). Therefore, the Sequence 2 LST is also likely to be a laterally extensive, amalgamated complex of braided fluvial channels. The subsequent transgressive-regressive cycles are different to the TST-HST in Sequence 1, as they are representative of a far more significant relative sea level rise. The transgressive surface above the LST is representative of the regionally recognised Callovian Break-Up Unconformity. In the Petrel Sub-basin, the evidence suggests that this surface is not an erosional boundary, but is representative of a change in the sedimentary depositional character from aggradational LST to retrogradational TST. O'Brien *et al*. (1993) noted that in the Vulcan Sub-basin to the northwest of the Petrel Sub-basin, the Callovian Break-Up Unconformity is represented by a rapid marine transgression, which quickly flooded the grabens. The increase in relative sea level resulted in a shallow marine influence, and the cored intervals at Gull-1 and Petrel-1 were interpreted as delta plain to shoreface deposits. Therefore, the relatively homogeneous, amalgamated fluvial sandstones of the LST were

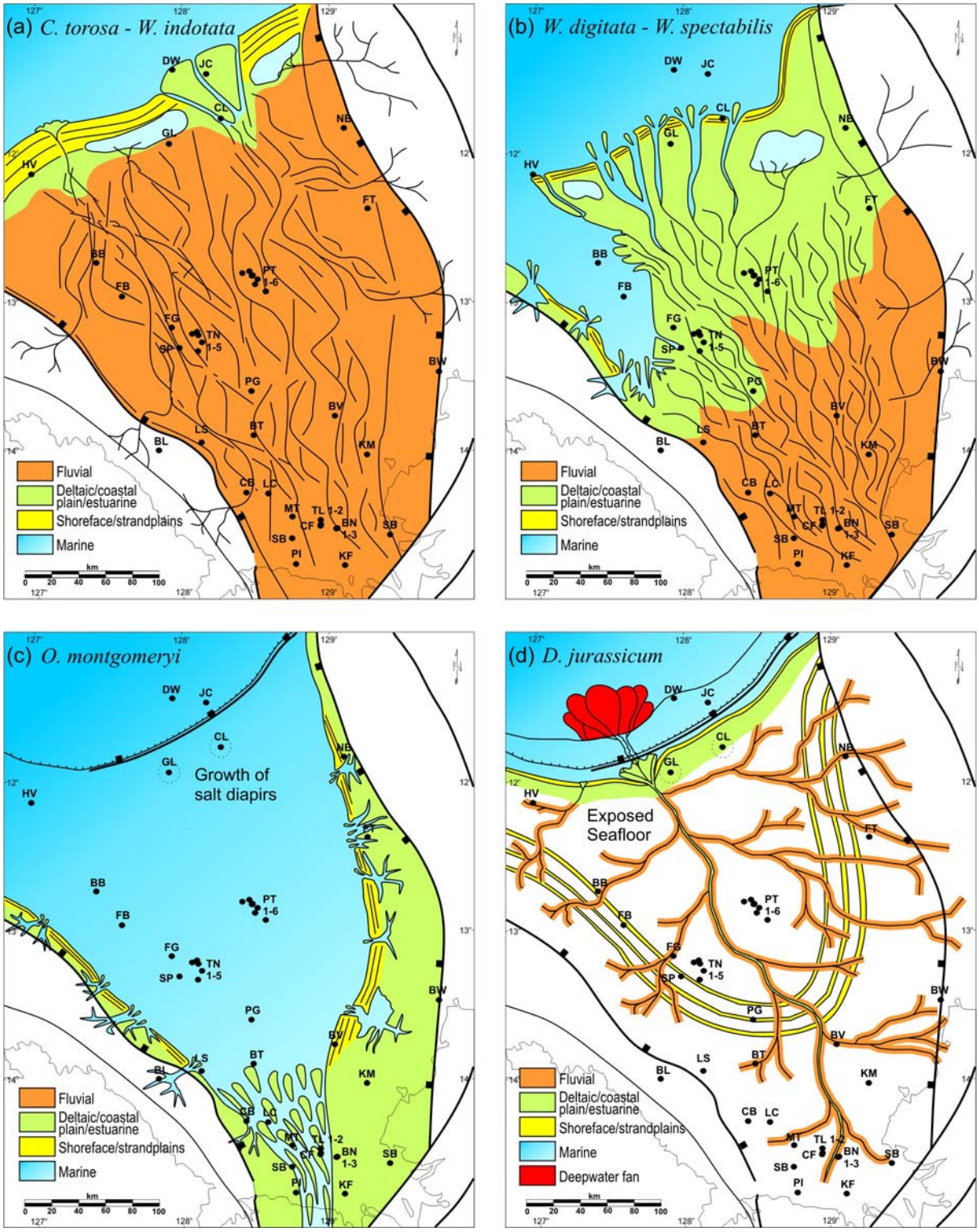

Figure 5.22 Series of regional palaeogeography maps, highlighting the different depositional environments at various points in time through the sequence stratigraphic interpretation.
(a) Sequence 1 to Sequence 2 LST, *C. torosa–W. indotata*, Plover Formation: braid plain to braid delta. (b) Sequence 2 TST/HST, *W. digitata–W. spectabilis*, Elang Formation: coastal plain, delta plain and interdistributary bay. (c) Sequence 3 maximum flooding surface, *O. montgomeryi*, lower Frigate Formation: estuarine embayment to marine shelf. (d) Sequence 4 LST, *D. jurassicum*, middle Frigate Formation: forced regressive shorefaces, exposed shelf, lowstand delta and deepwater fan.

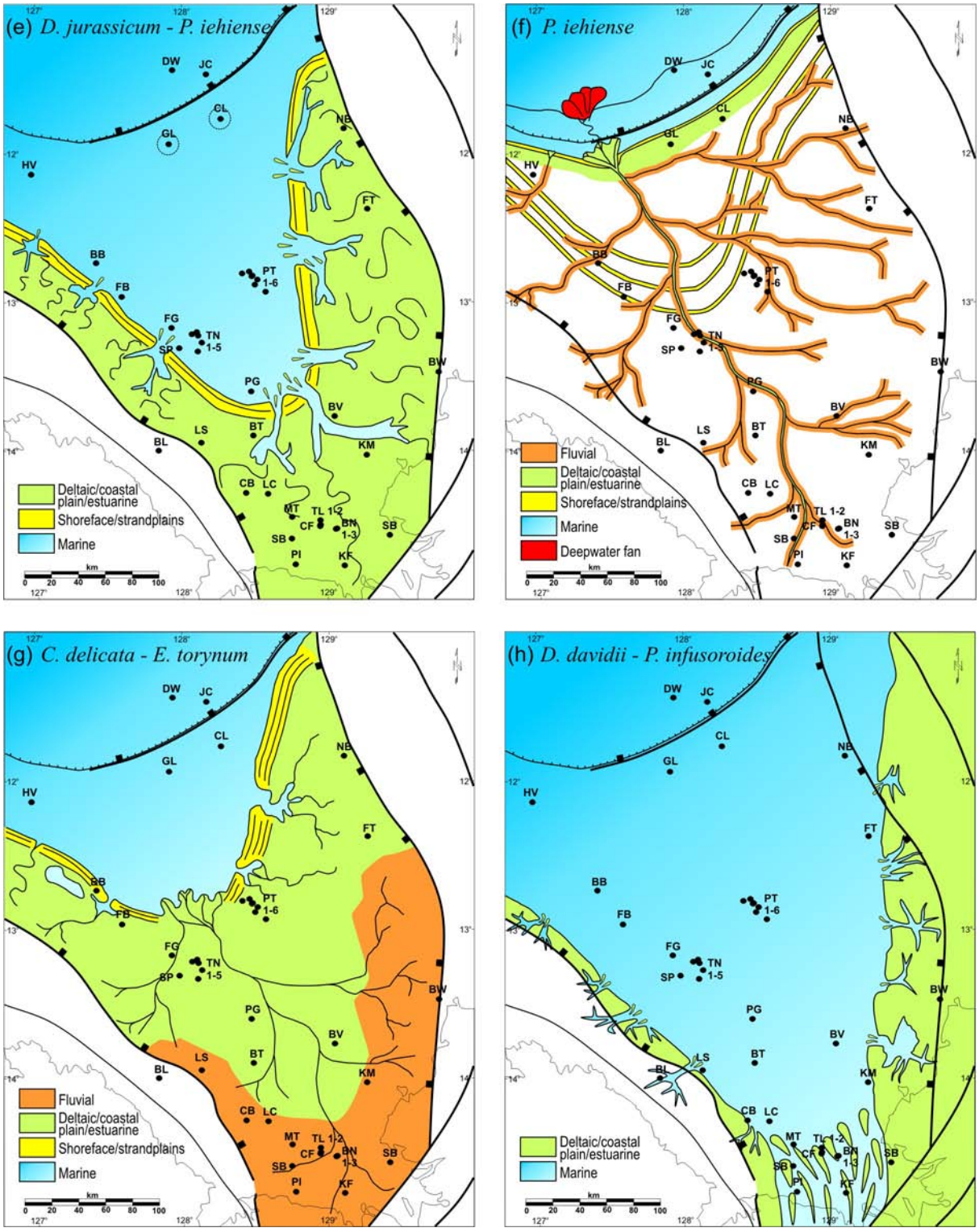

Figure 5.22 Series of regional palaeogeography maps, highlighting the different depositional environments at various points in time through the sequence stratigraphic interpretation.
(e) Sequence 4 TST/HST, *D. Jurassicum–P. iehiense*, upper Frigate Formation: estuarine embayment, lower shoreface and marine shelf. (f) Sequence 5 LST, *P. iehiense*, lower Sandpiper Sandstone: forced regressive shorefaces/strandplain, lowstand delta and deepwater fan. (g) Sequence 6 HST, *C. delicata–E. torynum*, upper Sandpiper Sandstone: coastal plain, shoreface to marine shelf. (h) Sequence 8 HST, *D. davidii–D. multispinum/P. infusoroides*, Bathurst Island Group: estuarine embayment to marine shelf.

replaced by more heterogeneous deltaic sandstones (increased number of shale breaks) in the following TSTs and HSTs (Figure 5.22b).

5.5.3.3 Sequence 3

Sequence 3 does not contain a LST in the area studied, but instead comprises a transgressive-regressive cycle of TST and HST. The sequence spans the *D. swanense* to early *D. jurassicum* palynological zones and is representative of the lower Frigate Formation. Although the seismic data suggest that the lower Frigate Formation only extends across the central and southern part of the basin, the well logs and biostratigraphy indicate that a very thin succession is present in the north, but is below the seismic resolution. The much reduced thickness of the lower Frigate Formation over Gull-1 and Curlew-1 is likely to be due to salt movement at the time of deposition (both wells are sited over salt diapirs) (McConachie *et al.*, 1995). The base of Sequence 3 is identified from the well logs by a shift in the GR wireline log motif, from a progradational, low GR signature to an increasing GR, retrogradational (transgressive) trend. On both the well logs and seismic sections, Sequence Boundary 3 does not show evidence of being an erosional contact, however, the palynological data indicate a hiatus in deposition with the absence of the *W. clathrata* zone. Sequence Boundary 3 is representative of the regionally recognised Tithonian Unconformity. The TST is represented on the well logs by a sandstone to shale, retrogradational stacking pattern, followed by an aggradational to progradational HST. The strong retrogradational character of the wireline logs over the first TST is reflected in the seismic as a back-stepping seismic facies (Figure 5.9, Figure 5.18–Figure 5.21).

There are no cored intervals through Sequence 3; however, the cuttings descriptions indicate that the unit is dominated by grey, soft to firm, partly glauconitic and micaceous claystone/shale, associated with argillaceous siltstone. The fine-grained nature of the rocks and high GR log motif suggest a marine shelf environment of deposition, which is supported by evidence from the palynology of a number of well completion reports, which noted the presence of marine microplanktons (Figure 5.22c).

5.5.3.4 Sequence 4

Sequence 4 does not contain a LST in the wells studied, but instead comprises two transgressive-regressive cycles of TST and HST. The sequence spans the late *D. jurassicum* palynological zone and is representative of the middle and upper parts of the Frigate

Formation. The first TST represents the middle Frigate Formation and extends across the majority of the basin, but is absent at Gull-1 and Curlew-1 (probably as a result of continuing salt diapirism). The following HST and 2nd cycle of TST-HST represent the upper Frigate Formation, which is only present over the central portion of the basin. It is interpreted that the upper part of Sequence 4 has been eroded over the rest of the basin by the subsequent Sequence 5. The base of Sequence 4 is identified on the well logs by a slight shift in the GR log motif to a retrogradational stacking pattern, representing the TST. This is followed on the well logs by an aggradational to progradational HST. The retrogradational-progradational stacking pattern is repeated for the 2nd cycle of TST-HST (Figure 5.18–Figure 5.21).

The absence of a LST in this sequence in the wells studied may be the result of sediment bypass. Robinson *et al*. (1994) have identified lowstand fans during this time period in the Malita Graben (at the northwest end of the Petrel sub-basin). In addition, down-stepping progradational sigmoid seismic facies are seen on the seismic between the Petrel Field and Bougainville-1 (Figure 5.9). These are interpreted to represent lowstand forced regressive shorelines, but the lack of well information in this area means this interpretation of the seismic cannot be clarified. Therefore, only the TST and HST cycles are represented in the wells in the central Petrel Sub-basin. The cored interval within this sequence at Petrel-1 was interpreted as lower shoreface to shelf depositional environment. However, near the southern margin at Bougainville-1, and towards the eastern margin at Flat Top-1, the cuttings descriptions and wireline log character indicate that the unit has become dominantly sandy. Thus, the lower shoreface and shelf siltstones and shales seen in the north and centre of the basin become sandy shoreface sands up-dip towards Bougainville-1 (Figure 5.22 d and e).

5.5.3.5 Sequence 5

Sequence 5 comprises a LST with a thin TST and HST. The palynological resolution is poor over the upper part of this interval, but it is thought that the sequence spans the *P. iehiense* to *K. wisemaniae* palynological zones. The sequence represents the lower Sandpiper Sandstone and is present across the central and northern part of the basin but is absent in the south. The base of Sequence 5 is identified from the well logs by a distinct change in the GR wireline log motif, from high GR signature suggestive of siltstones and mudstones, to a sharp-based, low GR signature, indicative of a basinward shift in facies. The LST is characterised in the well logs by a sharp-based sandstone that varies in thickness. The central and northern wells have a moderately thick LST, whereas the wells to the west have

only a thin LST. The TST is represented by a very thin retrogradational stacking pattern, with a moderately thick aggradational to progradational HST above (Figure 5.18–Figure 5.21).

A down-stepping prograding sigmoidal seismic character is observed on the seismic to the northwest of Petrel-1 and is a reflection of falling relative sea level and the development of a forced regressive shoreface during the LST (Figure 5.9). Depending on the degree of attachment of the forced regressive shorelines, the reservoir interconnectivity could range from moderate to excellent considering the sand-prone nature of the interval (Figure 5.22f).

5.5.3.6 Sequence 6

Sequence 6 comprises a LST, with a very thin TST and moderately thick HST and spans the *K. wisemaniae* to *E. torynum* palynological zones. The sequence represents the upper Sandpiper Sandstone. The LST is present across the central and northern part of the basin but is absent in the south, whereas the TST and HST are present across the whole area of interest. The base of Sequence 6 is identified on the well logs by a return to a low GR wireline log motif. The LST is represented by a low GR, aggradational stacking motif, followed by a very thin retrogradational TST, subsequently overlain by an aggradational to progradational HST (Figure 5.9, Figure 5.18–Figure 5.21). The cored interval at Gull-1 was interpreted as a middle to lower shoreface environment of deposition (Figure 5.17). It is most likely these represented linear shorelines striking in a crescent shape across the Petrel Sub-basin, representing infilling from both the southwest and southeast (Figure 5.22g).

5.5.3.7 Sequence 7

Sequence 7 does not contain a LST, but instead comprises a thin transgressive-regressive cycle of TST and HST. The sequence spans the *S. tabulata* to *A. cinctum* palynological zones. The sequence is representative of the Echuca Shoals Formation and extends across the whole area of interest. The base of Sequence 7 is identified from the well logs by a shift in the GR wireline log motif, from a low GR signature to an increasing GR, retrogradational (transgressive) trend. The well logs do not show evidence of an erosional contact, however, the palynological data indicate a hiatus in deposition with the absence of the *S. areolata* zone. Sequence Boundary 7 is representative of the regionally recognised Valanginian Unconformity. The TST is represented by a thin retrogradational sandstone to shale package, overlain by a thin progradational HST (Figure 5.18–Figure 5.21).

Sequence 7 is a condensed interval associated with a rapid rise in relative sea level, with several palynological zones compressed within a thin sedimentary succession. There are no cored intervals through Sequence 7; however, from the cuttings descriptions the unit is dominantly described as glauconitic claystone/shale, with associated very fine- to fine-grained glauconitic sandstone. The fine-grained nature of the rocks suggests a marine shelf environment of deposition, which is supported by presence of marine microfossils noted in a number of well completion reports. The sequence represents a drowning of the previous coastal system and suggests there was also a significant reduction in sediment supply (Figure 5.22h).

5.5.3.8 Sequence 8

Individual systems tracts have not been identified in Sequence 8, as both the wireline log motifs and seismic show very little variation. The sequence extends from the *D. davidii* palynological zone and up through the Cretaceous, to approximately *D. multispinum*/*P. infusorioides*. The base of Sequence 8 is identified from the well logs by a distinct increase in the sonic wireline log motif (Figure 5.18–Figure 5.21), and on the seismic as the surface which separates high amplitude sub-parallel reflectors of the upper Sandpiper Sandstone from the low amplitude large-scale progrades of the Bathurst Island Group (Figure 5.9). On both the well logs and the seismic, Sequence Boundary 8 does not show evidence of being an erosional contact, however, the palynological data indicate a hiatus in deposition with the absence of the *O. operculata* zone. Sequence Boundary 8 is representative of the regionally recognised Aptian Unconformity. Sequence 8 can essentially be characterised as a supersequence HST, with an aggradational to progradational stacking pattern (Figure 5.9, Figure 5.18–Figure 5.21). The cored intervals within Sequence 8 at Gull-1 and Petrel-1 were interpreted as offshore marine shelf deposits (Figure 5.17), which, in conjunction with the large-scale prograding clinoforms seen on the seismic, are thought to represent shelf-scale progradation (Figure 5.22h).

5.6 INJECTIVITY

Upon injection into a reservoir rock, the flow behaviour and migration of CO_2 will depend primarily on parameters such as the injection rate, viscosity ratio and relative permeability, but is also influenced by the stratigraphic architecture, reservoir heterogeneity and structural configuration of the rocks. Factors affecting injectivity that can be assessed through the

geological characterisation therefore include the reservoir's quality, geometry and connectivity.

5.6.1 Reservoir Quality

5.6.1.1 Porosity and Permeability

Core plug porosity and permeability data are very limited over the intervals of interest, and the data that is available shows a range of reservoir quality (Figure 5.23 and Appendix D). The Plover and Elang formation sediments have porosities ranging up to 24 % and permeabilities ranging up to 900 mD. However, the majority of the core data points are less than 15 % porosity and 100 mD permeability, indicating moderate reservoir quality. The overlying Sandpiper Sandstone exhibits similar reservoir quality.

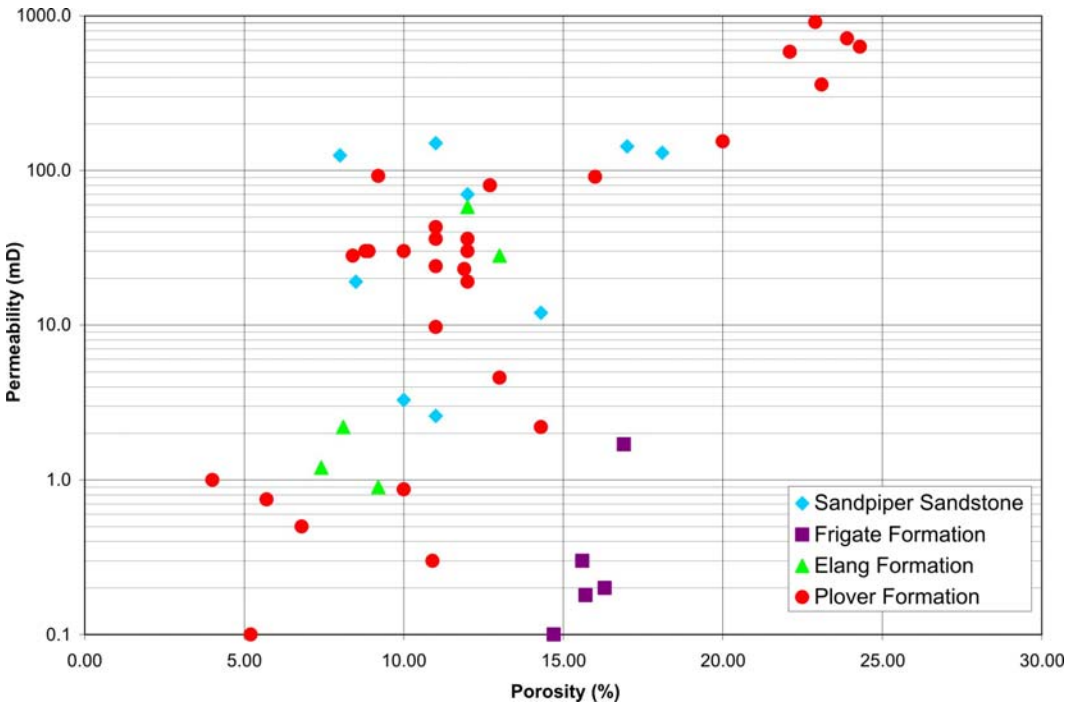

Figure 5.23 Core plug porosity and permeability data from Gull-1 and Petrel-1, discriminated by formation.

Calculated wireline log porosity and permeability over the full reservoir intervals were estimated by the petrophysics interpretation (Skinner, 2000). The petrophysical analysis of the wireline logs indicated that the reservoir quality of both units was moderate to very good. Porosity ranges between 8–25 % (average 19.1 %) and permeability ranges between 4–1122 mD (average 285 mD) for the Plover/Elang formations, and for the Sandpiper Sandstone porosity ranges between 13–25 % (average 21.5 %) and permeability ranges between 73–

3656 mD (average 1673 mD) (Table 5.3). The slightly decreased reservoir quality in the Plover/Elang formations in comparison to the Sandpiper Sandstone is most likely just due to the deeper depth of burial.

Table 5.3 Wireline log-derived reservoir property averages for the Plover/Elang formations and Sandpiper Sandstone (after Skinner, 2000).

5.6.1.2 Petrographic Characterisation

A petrographic assessment, including thin section description, modal composition analysis, X-ray diffraction bulk/clay mineralogy and scanning electron microscopy (SEM), was conducted on selected core samples from Gull-1 and Petrel-1 (Kraishan, 2000). The pore-scale petrographic characterisation determined that the framework composition of all the

Petrel Sub-basin sandstone samples is predominantly monocrystalline quartz, with minor to trace amounts of feldspar, metamorphic and sedimentary rock fragments, and polycrystalline quartz. The Plover and Elang formations are classified as quartz arenite, subarkose and sublitharenite and the Sandpiper Sandstone is classified as quartz arenite and subarkose (Figure 5.24). The minor feldspar component comprises mostly orthoclase and microcline. Plagioclase feldspar (in the form of albite) occurs rarely. Schist, metaquartzite and chert are the main lithic fragments but siltstone and claystone also occur in trace amounts. Muscovite is present in trace to minor amounts and is slightly altered in the studied samples, either disseminated or concentrated in very thin lamellae parallel to the bedding planes. The heavy mineral suite includes tourmaline and zircon. Dispersed organic matter is minor in the samples and comprises coalified wood and plant materials. Detrital matrix is present in trace to minor amounts in most of the samples, which supports the sedimentological interpretation of a moderate to high-energy depositional environment (Kraishan, 2000).

Figure 5.24 QRF ternary diagram showing framework grain composition of the Petrel Sub-basin sandstones. The axes of the diagram are: quartz (Q) = 100%, feldspars (F) = 50% and rock fragments (R) = 50% (modified after Kraishan, 2000).

Authigenic phases are dominated by quartz overgrowth cement, which occurs as thin to occasionally thick, euhedral overgrowths (Figure 5.25). Kaolinite cement is common in many samples and occurs as pseudo hexagonal book-like crystals filling many of the pore spaces and locally restricting the reservoir quality (Figure 5.25). Illite clay is also present and occurs as fibrous to hairy crystals filling, bridging the pore spaces and pore throats (Figure 5.25). In addition, illitic-smectite clay was sometimes present, occurring in the form of loose spherical rosettes filling some of the pore spaces and pore throats (Figure 5.25). Other more minor authigenic phases included ferroan carbonate cements (dolomite or ankerite), occurring as pore filling and as replacement phases, and siderite cement, occurring in a micritic form replacing organic-rich detrital matrix and in a sparry form developed locally around stylolites during chemical compaction (Kraishan, 2000).

The petrographical study revealed that visual porosity of the studied samples is poor to moderate at Gull-1 (average 10.2%) and moderate to good at Petrel-1 (average 17.9%). The visual porosity is dominantly primary intergranular porosity. Secondary porosity has mostly resulted from partial to complete dissolution of potassium feldspar. Both compaction and cementation processes have played significant roles in reducing the original intergranular porosity. In particular, extensive quartz cementation (as a result of increased depth) in both reservoir intervals at Gull-1 has reduced the pores and pore throat sizes, restricting the reservoir quality. In Petrel-1, the pores and pore throat sizes are much larger with good to very good interconnectivity, implying higher permeability and better reservoir quality. In summary, the reservoir potential of the studied samples is generally good. Many of the Petrel Sub-basin sandstones are matrix-poor and have fair to good reservoir characteristics; however, the quality of the reservoir sandstones are better developed at Petrel-1 than at Gull-1 (Kraishan, 2000).

5.6.1.3 Potential Impact of CO_2-Water-Rock Interactions on Reservoir Quality

CO_2 dissolution into the formation water allows CO_2-water-rock interactions, which will alter the mineralogy and potentially alter the physical aspects of the rock. This can have important implications for injectivity, as mineral dissolution may lead to migration of fine clay minerals and sand grains, or precipitation of new minerals, either of which can block or occlude the porosity and permeability of the reservoir rock.

The petrographic study indicated that the reservoir units of the Plover/Elang formations and Sandpiper Sandstone lack minerals that are reactive to CO_2. While rock fragments and

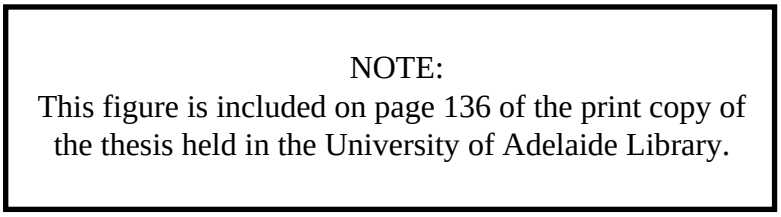

Figure 5.25 Selection of scanning electron microscope photomicrographs, highlighting reservoir quality of the Plover/Elang formations and Sandpiper Sandstone (modified after Kraishan, 2000).

feldspars do make up a minor component of the formation mineralogy, the chemical composition of each mineral group is not optimal for CO_2-water-rock interactions at a rate likely to affect injectivity. For example, the feldspars are dominantly alkali, which have a very slow reaction rate, and the rock fragments are metamorphic (quartz and mica dominated), which also have a very slow reaction rate or are inert to CO_2 dissolution (M. Watson, ASP, pers. comm.). The authigenic cement is predominantly quartz, thus dissolution of this cement by injected CO_2 is unlikely. The minor amounts of ferroan carbonate cement, however, could be subjected to dissolution if CO_2 is injected, thus locally increasing the injectivity potential. A potential risk to reservoir quality may occur where fibrous to hairy illite and fine kaolinite crystallites are present. During CO_2 injection, these fine minerals may migrate and block or fill pores and pore throats, thus possibly causing localised reductions in porosity and permeability.

5.6.2 Reservoir Geometry and Connectivity

The reservoirs of the Plover ESSCI, represented by Sequences 1 and 2, extend across the whole of the area of interest. The reservoir is thickest in the northwestern part of the basin, reaching a maximum thickness of approximately 1600 m, and thins towards the basin margins (southwest, south, southeast and east) (Figure 5.26). The average thickness of the reservoir over the centre of the basin (Petrel Field) is 450 m. Sequences 1 and 2 were interpreted as laterally extensive, braided fluvial to deltaic reservoir units. These are likely to have an overall excellent degree of interconnectivity due to the amalgamated nature of the braided channels, the typically sand-rich channel sediments and lack of preserved overbank sediments.

The reservoirs of the Sandpiper ESSCI, represented by Sequences 5 and 6, also extend across the whole of the area of interest. The reservoir is thickest at the north end of the basin, reaching a maximum thickness of approximately 650 m, and thins towards the basin margins (southwest, south and southeast) (Figure 5.27). The average thickness of the reservoir over the centre of the basin (Petrel Field) is 200 m. Sequences 5 and 6 were interpreted as shoreface to coastal plain reservoirs. The interconnectivity of these depend on the degree of detachment of the shorelines, but are thought to be moderate to excellent considering the sand-prone nature of the interval.

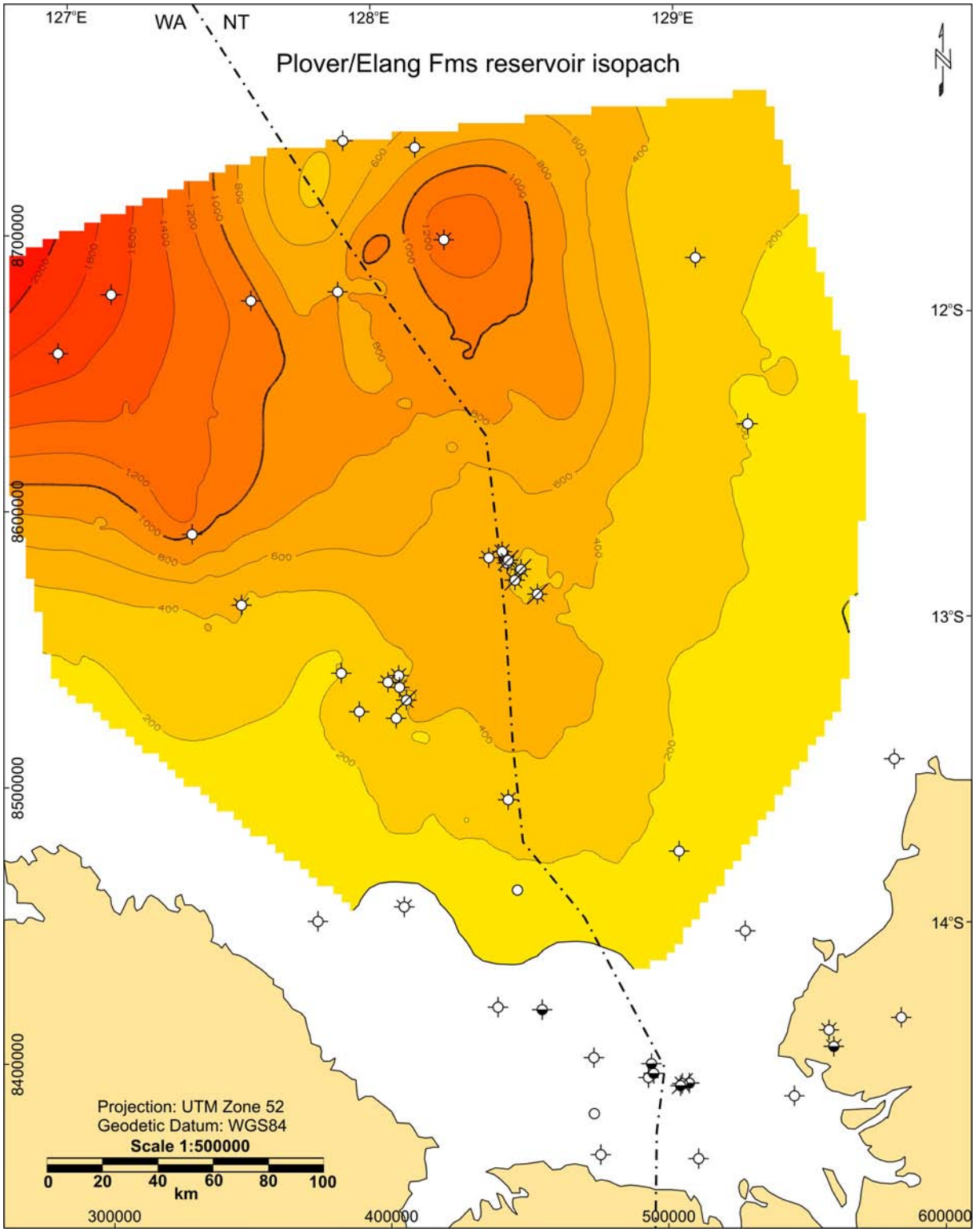

Figure 5.26 Isopach map of the Plover and Elang Formation reservoir, showing increasing thickness to the northwest.

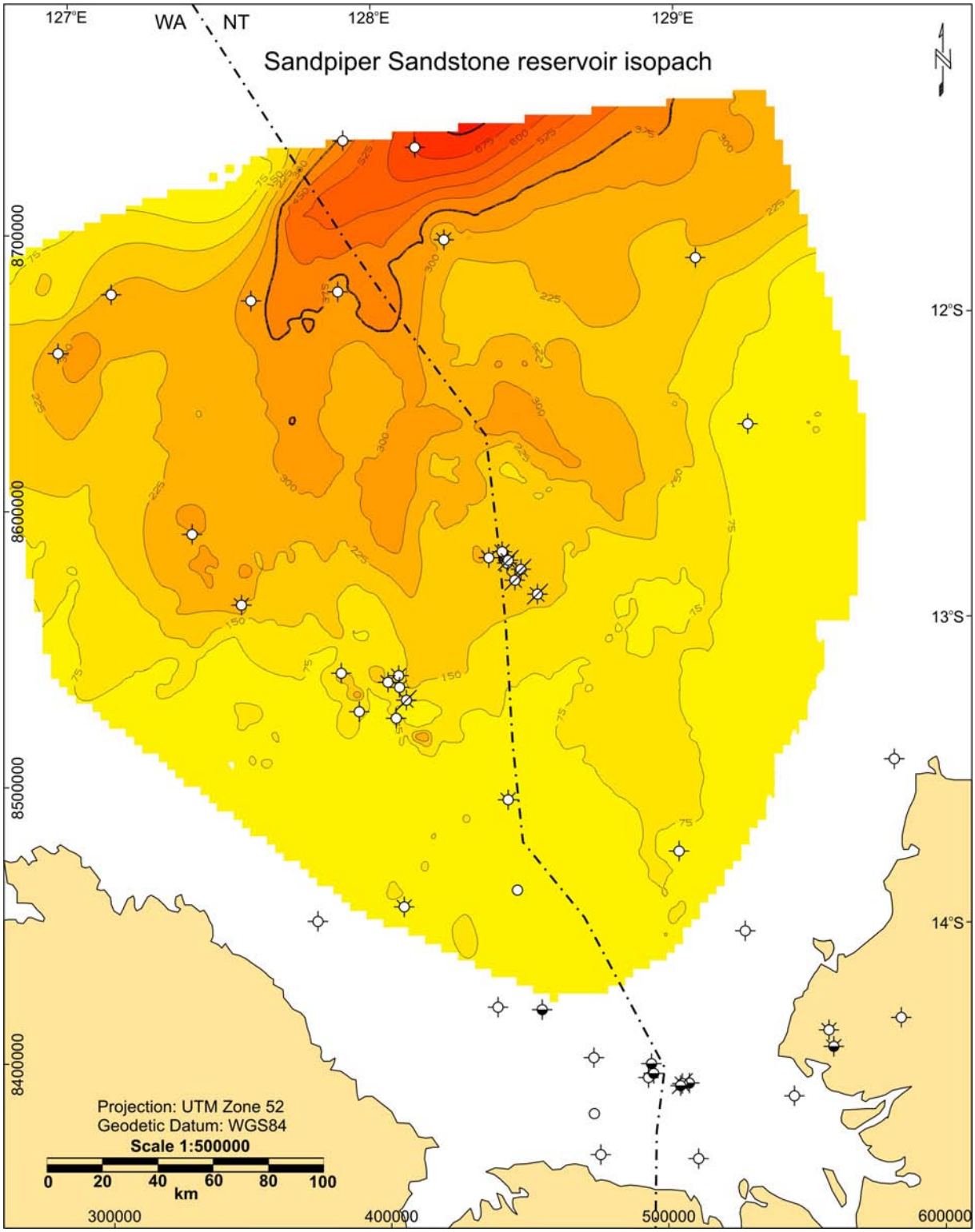

Figure 5.27 Isopach map of the Sandpiper Sandstone reservoir, showing increasing thickness to the north.

5.7 CONTAINMENT

Supercritical CO_2 is less dense than water (before dissolution); therefore, it will rise buoyantly through the water column. Consequently, containment could be breached by unwanted vertical fluid migration through the top seal, faults/fractures and existing well penetrations. Containment issues that can be assessed through the geological characterisation therefore include the extent, continuity and capacity of the seal, the likely migration pathways and trapping mechanisms, and the geomechanical integrity of the reservoir and seal.

5.7.1 Seal Distribution and Continuity

The Frigate Formation seal to the Plover/Elang reservoir formations (Sequences 3 and 4) extends across the majority of the study area, but at seismic resolution becomes absent to the north over Gull-1 and Curlew-1, although the well logs and biostratigraphy indicate that a thin succession is still present. The movement of salt at Gull-1 and Curlew-1 at the time of deposition probably caused the thinning of the sequence in the northern part of the basin (McConachie *et al.*, 1995). The seal is thickest over the Petrel Field location, reaching a maximum of approximately 330 m, and thins towards the basin margins (southwest, south and southeast) and to the north (Figure 5.28). According to the sequence stratigraphic interpretation, the lower shoreface and shelf siltstones and shales, seen in the north and centre of the basin, may become coarser shoreface sandstones up-dip towards Bougainville-1 and Flat Top-1. Therefore, due to the lateral facies change towards the south and east, the Frigate Formation is unlikely to completely seal the underlying reservoirs of the Plover and Elang formations across the whole of the study area and there is potential for migration of CO_2 into the overlying Sandpiper Sandstone.

The Bathurst Island Group regional top seal (Sequences 7 and 8) extends across the entire study area. Although the Bathurst Island Group extends to the Cretaceous/Tertiary boundary, it was thought somewhat unrealistic to treat the entire succession as regional seal, so a prominent seismic reflector within the succession was chosen as the ‘top’ of the sealing unit. Thus, the seal thickness and extent may actually be of greater proportions than depicted here. The seal is thickest in the northwest part of the basin, reaching a maximum thickness of approximately 1000 m, and thins towards the basin margins (southwest, south and east) to less than 100 m (Figure 5.29). The average thickness of the regional seal over the centre of the basin (Petrel Field) is 700 m. The unit is dominantly described from cuttings descriptions as a grey, micaceous, glauconitic, partly silty mudstone, with thin stringers/interbeds of micritic or

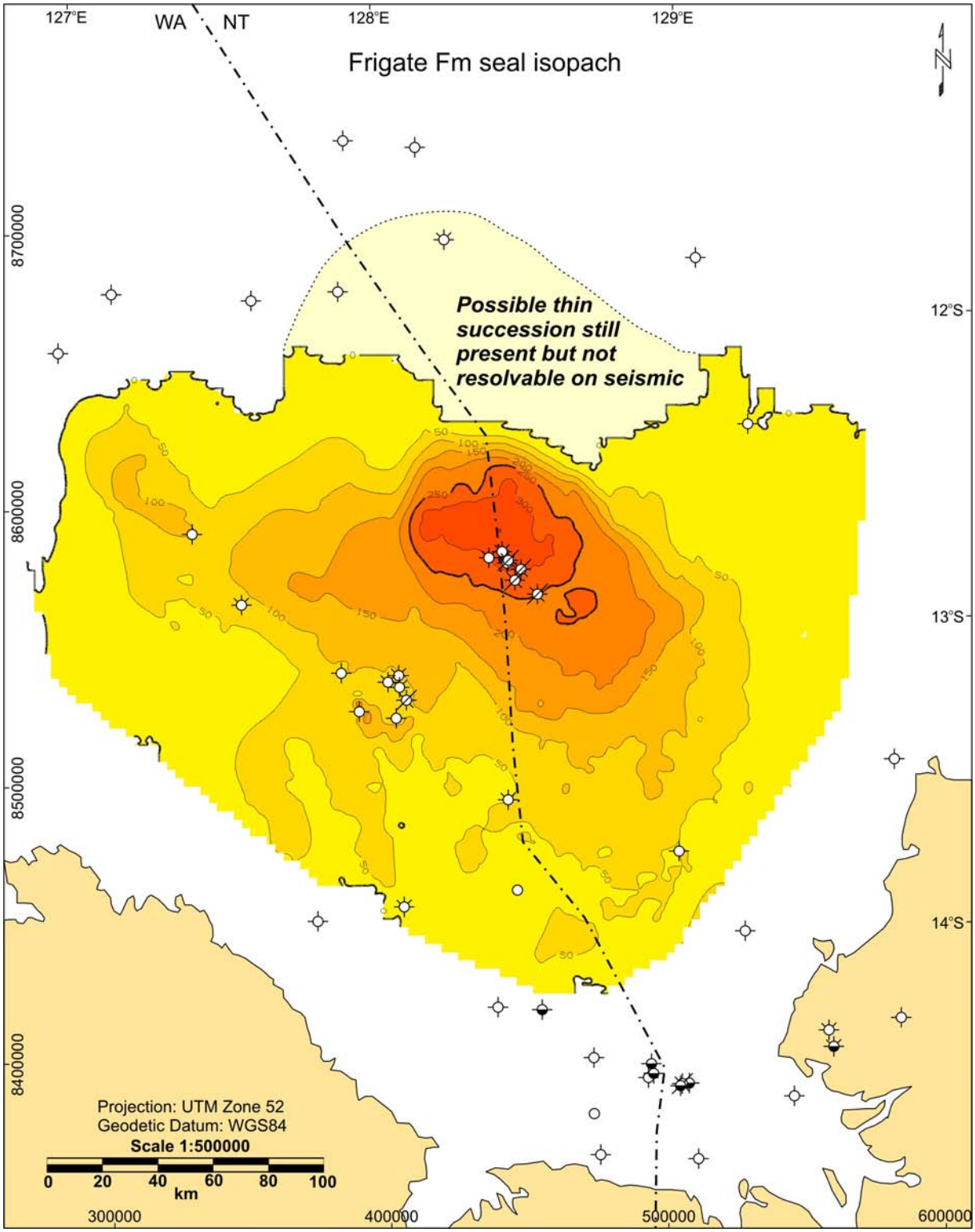

Figure 5.28 Isopach map of the Frigate Formation seal in between the Plover and Sandpiper ESSCIs, showing the seal is thickest over the Petrel Field location.

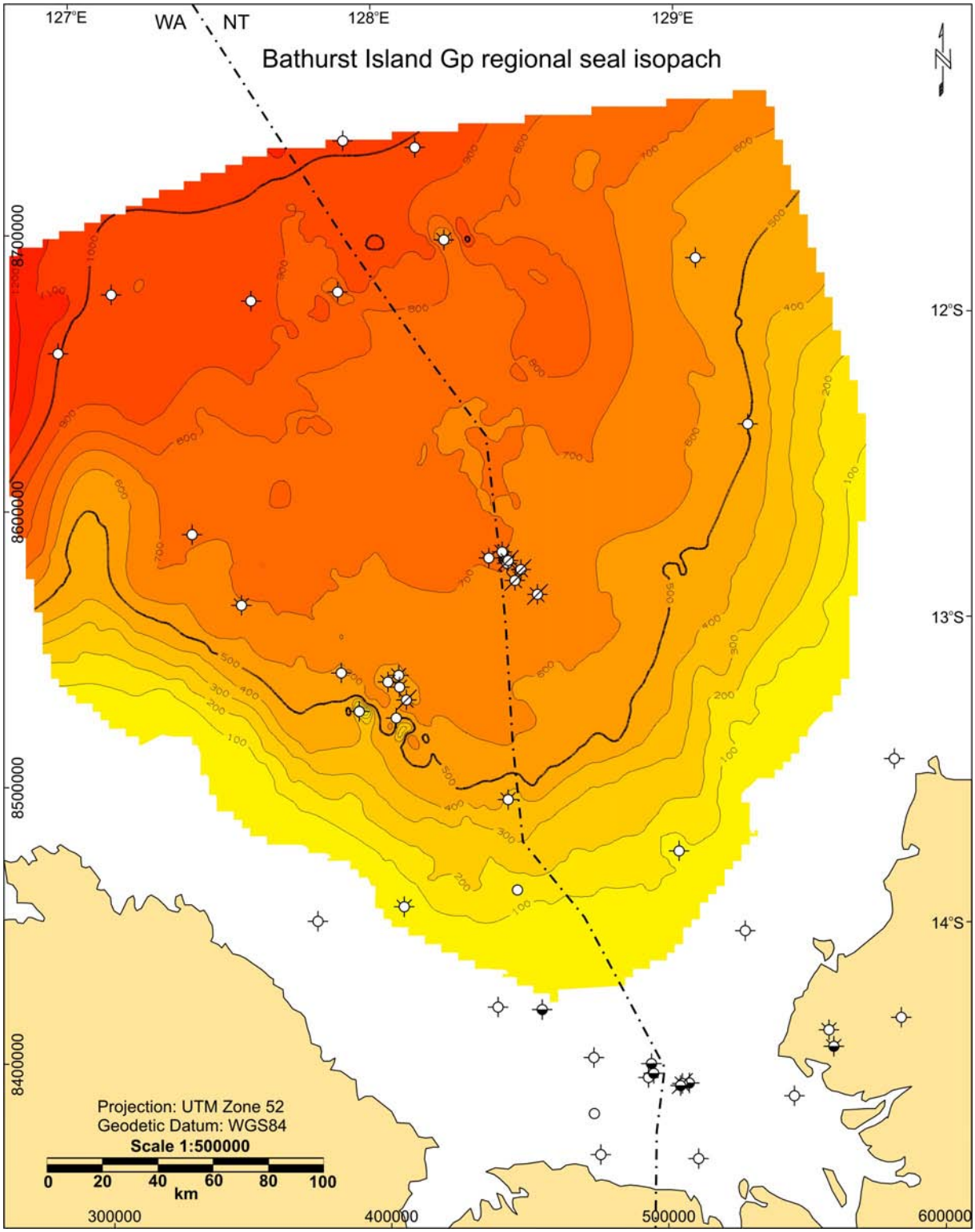

Figure 5.29 Isopach map of the Bathurst Island Group regional seal, showing increasing thickness to the northwest.

densely crystalline limestone. Vertically, above the seismically interpreted 'top' of the Bathurst Island Group, the lithology of this unit becomes siltier and sandier towards the Cretaceous/Tertiary boundary. The Bathurst Island Group is therefore interpreted, on the basis of lateral extent and lithology, to provide a suitable regional seal to the Sandpiper ESSCI and underlying Plover ESSCI. The only potential risk to loss of containment from this seal is from the thinning of the unit around the basin margins.

5.7.2 Seal Capacity

The maximum CO_2 column height that a seal is capable of retaining is an important aspect for assessing the quality of the seal. The potential seal capacity of the Frigate Formation and the Bathurst Island Group were calculated using mercury injection capillary pressure (MICP) analysis. MICP tests are a measurement of the pressures required to move mercury through the pore network system of a core sample. Using the techniques described earlier in Chapter 3, the mercury/air capillary pressure data were translated to equivalent CO_2/water data at reservoir conditions and then converted into seal capacity for CO_2, expressed as the column height that the rock would be capable of holding (sealing). Figure 5.30 shows examples of the mercury intrusion graphs for three of the seal samples, indicating the interpreted threshold pressure points (the mercury intrusion graphs for all samples are shown in Appendix E). The calculated column heights for each of the samples tested are listed in Table 5.4.

Table 5.4 CO_2 column heights calculated from MICP analysis.

Well Name	Depth TVDSS (m)	Press. (MPa)	Temp. (°C)	CO_2 Density (g/cm^3)	Brine Density (g/cm^3)	Interfacial Tension (mN/m)	Seal P_{th} Hg-air (psia)	Seal P_{th} CO_2-H_2O (psia)	Column Height (m)
Gull-1	1522.50	15.2	71.7	0.4997	0.9995	27.58	2947.41	221.08	310
Gull-1	1523.18	15.2	71.7	0.4997	0.9995	27.58	2932.14	219.93	309
Gull-1	1817.45	18.2	81.7	0.5337	0.9948	27.23	7074.48	523.90	799
Gull-1	2195.90	22.0	94.5	0.5565	0.9881	26.50	101.59	7.32	11
Petrel-1	723.86	7.2	45.4	0.1920	1.0096	36.58	2062.97	205.23	176
Petrel-1	726.91	7.3	45.5	0.1968	1.0096	36.19	2925.85	287.97	249
Petrel-1	1028.21	10.3	56.1	0.3394	1.0059	29.75	2949.25	238.62	251
Petrel-1	1029.49	10.3	56.1	0.3394	1.0059	29.75	2059.64	166.64	175
Petrel-1	1029.73	10.3	56.1	0.3394	1.0059	29.75	2934.45	237.42	250
Petrel-1	1553.60	15.5	74.5	0.4893	0.9980	27.72	340.76	25.69	34

Note: P_{th} = threshold pressure; Salinity = 32189 ppm; contact angle = 0°; reservoir P_{th} Hg-air system = 6.85 psia.

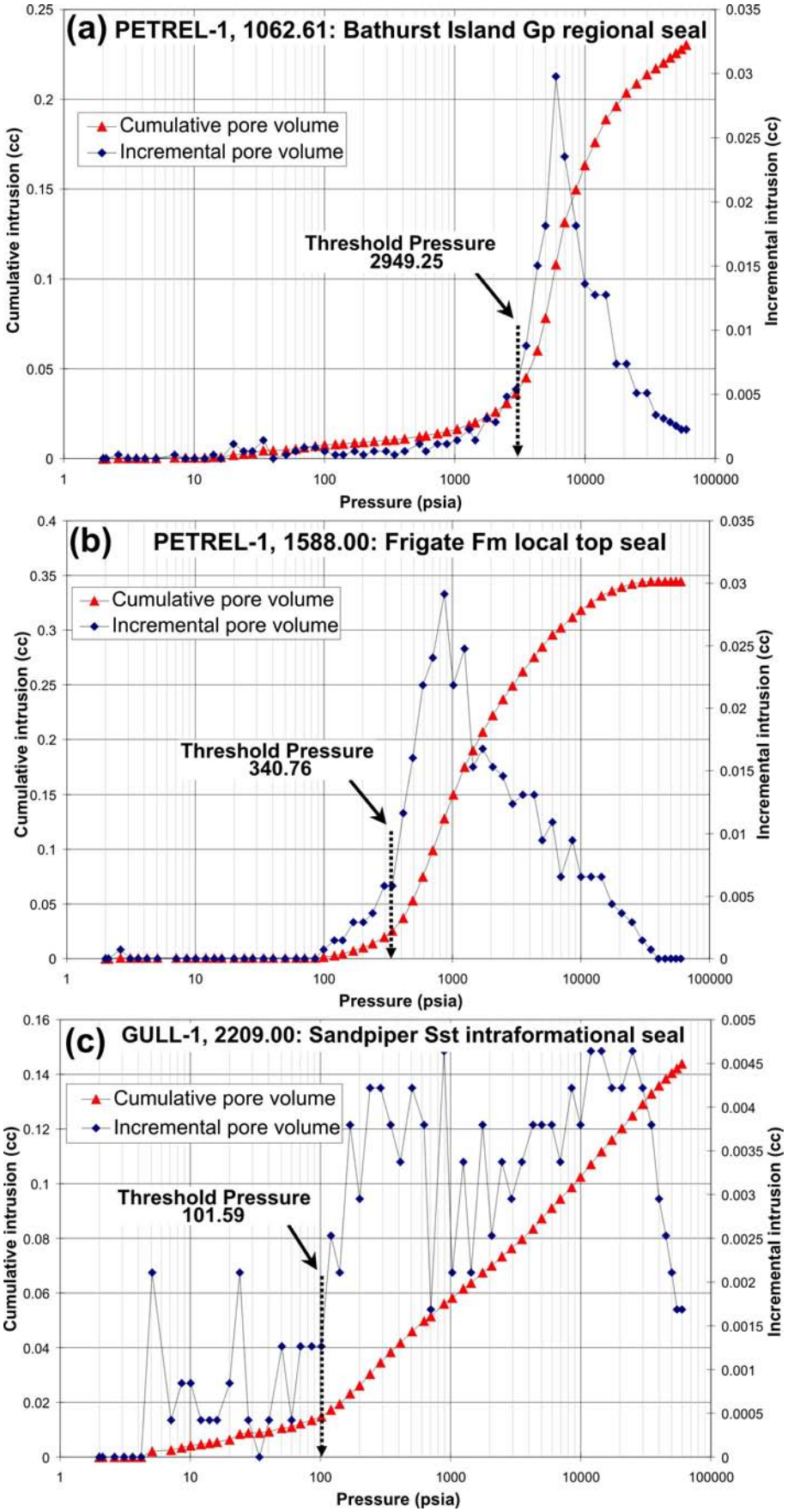

Figure 5.30 Example mercury injection capillary pressure curves highlighting threshold pressure for: (a) Bathurst Island Group regional seal; (b) Frigate Formation local seal; and (c) intraformational seal.

The results of the MICP analyses indicate that the Bathurst Island Group has good to excellent seal capacity, with the potential to hold back CO_2 column heights ranging from 175 m to 800 m. The average CO_2 column height retention is 315 m. As there is no structural closure at the Sandpiper Sandstone reservoir level and the reservoir is generally less than 300 m thick, it is unlikely that a column of CO_2 greater than these proportions could ever occur; therefore, the seal capacity of the Bathurst Island Group is likely to be more than sufficient to successfully retain CO_2 beneath it. In comparison, the Frigate Formation seal to the underlying Plover and Elang formations has quite poor seal capacity, with a maximum CO_2 column height retention of only 34 m. However, the cored section of the Frigate Formation was taken from a sandier part of the succession, therefore, it is possible that the shalier parts of the Frigate Formation could potentially hold back CO_2 column heights greater than 34 m. A thin siltstone layer (~2 cm thick) within the Sandpiper Sandstone reservoir was calculated to hold a CO_2 column height of 11 m. Therefore, heterogeneities such as these within the reservoir units are unlikely to be significant barriers to flow but could provide minor baffles that would hinder or slow the vertical migration of CO_2.

5.7.3 Migration Pathways and Trapping Mechanisms

After injection ceases, the buoyancy of the free-phase (immiscible) CO_2 due to its density will result in it migrating to the highest point in the reservoir. Stratigraphic heterogeneities, such as intraformational siltstones and shales, have the potential to reduce the effective vertical permeability and create a more tortuous migration pathway for injected CO_2. Once CO_2 has reached the top of the reservoir, the structural dip and geometry at the base of the overlying seal will have a strong influence on the subsequent migration direction.

The structural geometry of the reservoirs and seals of the Petrel Sub-basin was evaluated through the seismic interpretation, discussed earlier in section 5.4.1. The general structural trend of the strata, with the exception of areas immediately adjacent to salt diapers, is a gentle slope dipping up towards the basin margins (southwest, south and southeast), with a weakly developed, unclosed anticlinal structure trending along the basin axis in a northwest-southeast direction (Figure 5.11 and Figure 5.12). Flow vectors plotted on the base Bathurst Island Group regional seal depth surface indicate the up-dip migration directions based on the structural geometry (Figure 5.31). The exact positioning of an injection well will determine the ultimate migration direction of the CO_2. If an injection well is sited along the main axial trend of the basin, the effect of the tilted structural geometry suggests that CO_2 injected into

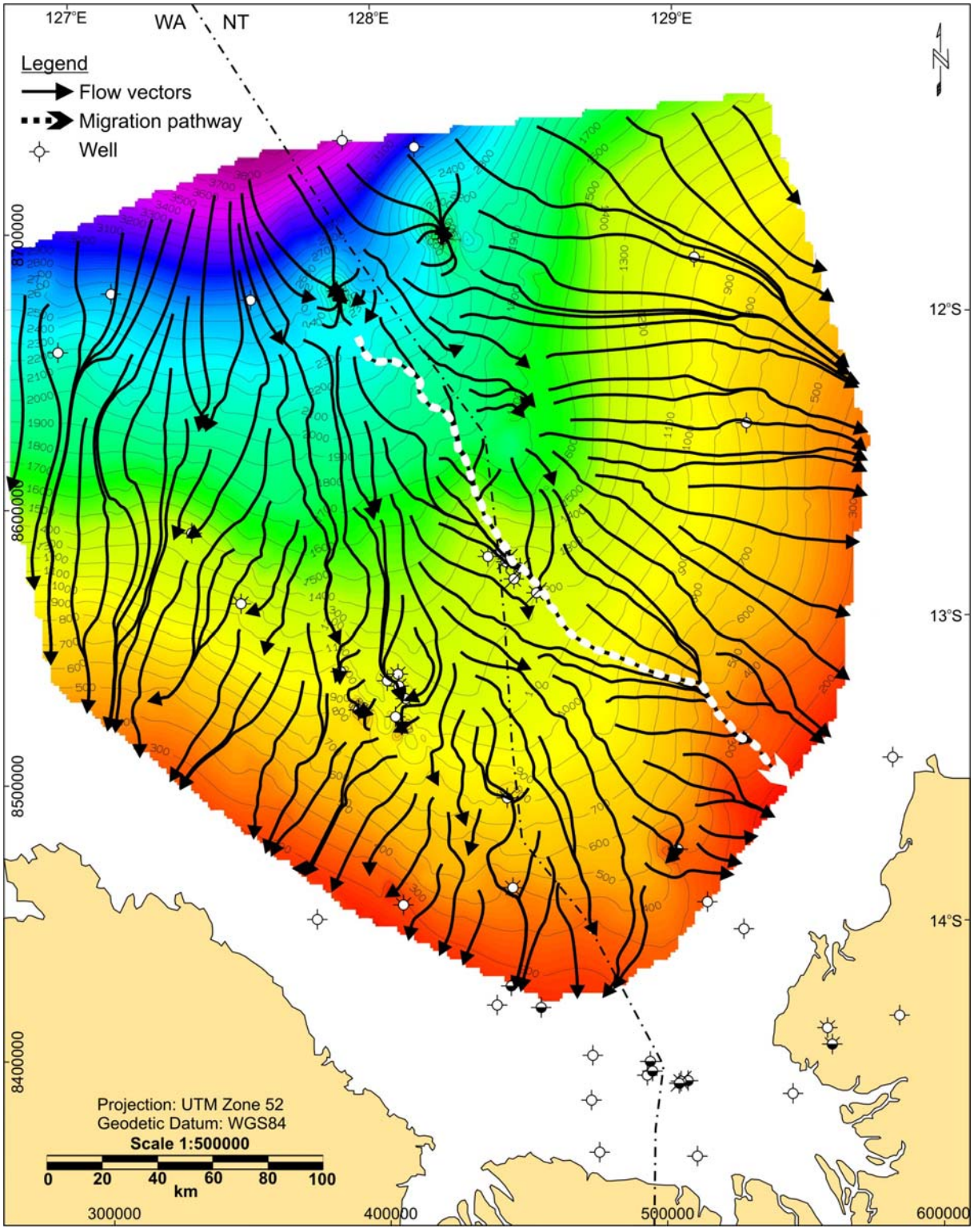

Figure 5.31 Potential CO_2 migration pathways based on the structural geometry of the Base Bathurst Island Group (base regional seal) depth structure surface. CO_2 migration is expected to occur along the axis of the basin towards the southeast if an injection site was located in the syncline between Gull-1 and Petrel-1. The actual migration pathway is dependent on the exact location of a potential injection site.

the Plover Formation is likely to migrate upwards and southeastwards until it reaches the top of the Elang Formation beneath the Frigate Formation seal. It will continue to migrate southeastwards beneath the Frigate Formation seal until it reaches the sandier shoreface section of the Frigate Formation, where breakthrough into the Sandpiper Sandstone reservoir may occur. Once in the Sandpiper Sandstone reservoir, the CO_2 will continue to migrate upwards and southeastwards beneath the Bathurst Island Group regional seal.

A suggested injection location would be in the syncline to the northwest of the Petrel Field (between Gull-1 and Petrel-1), which would give the longest possible migration distance before reaching the basin margins. The CO_2 would need to travel more than 100 km in all directions from an injection site in the syncline between the Petrel Field and Gull-1, before reaching the major basin-bounding faults or the thinner, more sandy regional seal. However, if the possibility of leakage up the existing well casings of the Petrel Field is considered too great a risk or there are economical constraints to having a 300 km pipeline, the recommended injection site would be just up-dip of the Petrel Field (southeast) along the same structural trend.

As there is no defined structural closure at both reservoir stratigraphic levels, CO_2 is unlikely to be trapped structurally, except for within minor bumps along the base of the seals. Stratigraphic trapping is also unlikely as the reservoir intervals are likely to become sandier and coarser-grained towards the basin margins. The dominant trapping mechanisms are therefore expected to be residual trapping along the migration pathway and dissolution into the formation water. Hydrodynamic trapping is likely if the residence time is sufficiently long (e.g. more than 1000 years before the edge of the seal or the basin-bounding faults are reached).

5.7.3.1 Potential for Mineral Trapping of CO_2

CO_2 introduced into the reservoir system will generate long-term CO_2-water-rock interactions. Detailed petrology can provide information on the potential mineral reactions of the CO_2 with the host rock, including dissolution, alteration and precipitation. In certain cases, mineral precipitation can lead to mineral trapping of CO_2 and increased containment security.

The petrographic characterisation by Kraishan (2000) determined the mineralogy of the Plover and Elang formations and the Sandpiper Sandstone reservoir units. As discussed above in section 5.6.1.3, the mineralogy of the reservoir units of the Petrel Sub-basin offer

little to no reactive potential with CO_2. Whilst this is beneficial in terms of not inhibiting injectivity, conversely it means that there is limited potential for mineralogical trapping of the CO_2 through precipitation of carbonate minerals.

5.7.4 Geomechanical Assessment of Fault Stability

CO_2 injection into the geological subsurface increases the formation pressure, which can potentially reactivate pre-existing faults or generate new fractures, leading to a possible loss of containment. Geomechanical modelling was undertaken by Streit (2001) to assess the stability of known faults in the Petrel Sub-basin. As noted earlier in section 5.4.2, the post-rift sediments in the Petrel Sub-basin are relatively unfaulted. However, the comparatively low fault density in the area does not preclude the potential for fault leakage.

The *in situ* stress regime in the Petrel Sub-basin is estimated to be transitional between a normal fault regime and a strike-slip fault regime, i.e. the maximum horizontal stress (S_{Hmax}) is equal to or greater than the vertical stress (S_v), which in turn is greater than the minimum horizontal stress (S_{hmin}) (Figure 5.32) (Streit, 2001). The orientation of the maximum horizontal stress is inferred to be consistent with S_{Hmax} orientations in other parts of the southern Bonaparte Basin and in the Timor Sea (varying from 040°N to 055°N) and a value of 050°N was used to approximate the S_{Hmax} direction (Mildren & Hillis, 2000; Streit, 2001).

The strike orientation of existing faults and their angle of dip with respect to the stress orientation and magnitude determine their potential for possible reactivation. The main faults that may be of concern are the large northwest-trending basin-bounding faults around the basin margins (Figure 5.3). These major faults are known to have steep dips of 60° to 70° (O'Brien *et al.*, 1993; O'Brien *et al.*, 1996). Reactivation of these faults within the inferred normal to strike-slip stress regime is unlikely if the actual stress regime is predominantly a normal fault regime. Some segments of these faults would permit reactivation if the stress regime favours strike-slip faulting (Figure 5.33) (Streit, 2001).

Other faults with west to west-northwest and north-northwest to north-northeast strike orientations also occur predominantly near the margins of the basin. Dip angles are not known for these faults, but their strike directions would permit reactivation with components of strike-slip movement within the inferred stress regime (Figure 5.33) (Streit, 2001). A few minor northeast-trending faults occur near the southwest margin of the basin and, although dip angles are again not known, the strike direction of these faults would permit their reactivation as normal faults within the inferred stress regime (Figure 5.33) (Streit, 2001).

Figure 5.32 Stress profile for the Petrel Sub-basin. Estimate of minimum horizontal stress (S_{hmin}) was based on pressure data from leak-off tests. Estimate of the vertical stress (S_v) was obtained by integrating data from density logs. Curves for frictional limits only give crude estimates for the magnitude of the maximum principle stress (S_{Hmax}) (modified after Streit, 2001).

Thus, the strike directions of west to west-northwest and north-northwest to north-northeast trending faults, as well as those of northeast-trending faults in the Petrel Sub-basin would permit their reactivation. It is noted that the majority of these faults occur near the southern margins of the basin outside the potential CO_2 containment area (the limit of the Bathurst Island Group regional seal). Although reactivation of some of the faults may be possible, this would only be induced if the appropriate pore fluid pressures required for failure were exceeded during injection. As only a limited geomechanical dataset is available for the Petrel Sub-basin, detailed prediction of pore pressure increase leading to fault reactivation cannot be estimated at this time (Streit, 2001).

5.7.5 Hydrodynamic Analysis of Formation Water Flow Systems

The existing formation water flow system within a geological reservoir may influence CO2 migration pathways and containment, both in terms of the magnitude of the fluid movement and the direction. Hydrodynamic modelling was undertaken by Bekele and Otto (2000) to assess the formation water flow systems operating within the Petrel Sub-basin.

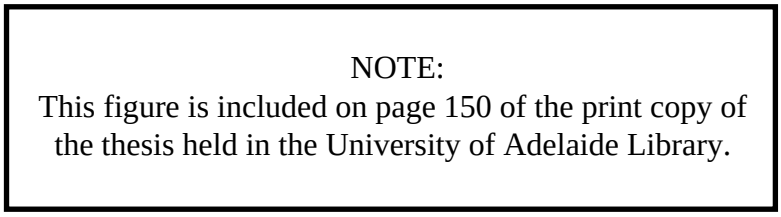

Figure 5.33 Map showing potential for fault reactivation in a normal or strike-slip stress regime: faults shown in blue are relatively stable and faults shown in red can possibly be reactivated (fault traces redrawn after Colwell & Kennard, 1996). Arrow indicates approximate S_{Hmax} direction. Faults to the south of the zero edge of the Bathurst Island Group regional seal isopach are outside the area of potential containment of CO_2 (modified after Streit, 2001).

The data set available for the hydrodynamic modelling was extremely limited; however, some important conclusions can be drawn from the results regarding the containment security of the Plover and Sandpiper ESSCIs. The general direction of the formation water flow within both the Plover/Elang formations and the Sandpiper Sandstone is towards the southeast, away from the depocentre and along the axis of the Petrel Sub-basin (Bekele & Otto, 2000). This is the same as the migration direction that the injected CO_2 is predicted to follow based on structural geometry and buoyancy drive. The speed of the formation water flow in the Plover Formation is estimated at 1 cm per year (Bekele & Otto, 2000), which is very slow (equivalent to 1 km per 100,000 years). The success of hydrodynamic trapping relies on the velocity of the formation water and the corresponding travel time to reach the edge of the overlying seal or other potential leak points. Therefore, the very slow flow velocity of the Plover Formation in conjunction with the considerable distance to the edge of the seal or basin-bounding faults (>100 km) should be of great benefit. The migration of the CO_2 will also be driven by buoyancy and by the increased pressure exerted by the injection rate, but the very slow flow velocity of the *in situ* formation water will aid the possible effectiveness of hydrodynamic trapping in the long-term and may increase the potential for residual and solubility trapping.

5.8 CAPACITY

To assess the potential CO_2 storage capacity, a 3D geological model was created from the structural and stratigraphic interpretations. The zones and layers of the model were constructed to reflect the internal stratigraphic architecture of the geological units seen on the seismic (Figure 5.34a). The 3D cellular grids were then populated with reservoir parameters derived from the petrophysical assessment (e.g. sand percent, porosity, permeability) using sequential Gaussian simulation (Figure 5.34b). Other physical parameters important to the behaviour of CO_2 (e.g. pressure, temperature) were also populated in the model. The cellular 3D geological models also provided the basis for the numerical flow simulation models of CO_2 injection and storage created during the engineering characterisation.

The results of the volumetric assessment for potential CO_2 storage capacity in the Plover and Sandpiper ESSCIs are presented in Table 5.5. As the potential accessible storage area encompasses the greater part of the basin depocentre, the volumetric calculations indicate that the Petrel Sub-basin has considerable available pore volume. However, not all of that available pore volume will be accessed by the CO_2 due to its buoyant nature. After initial

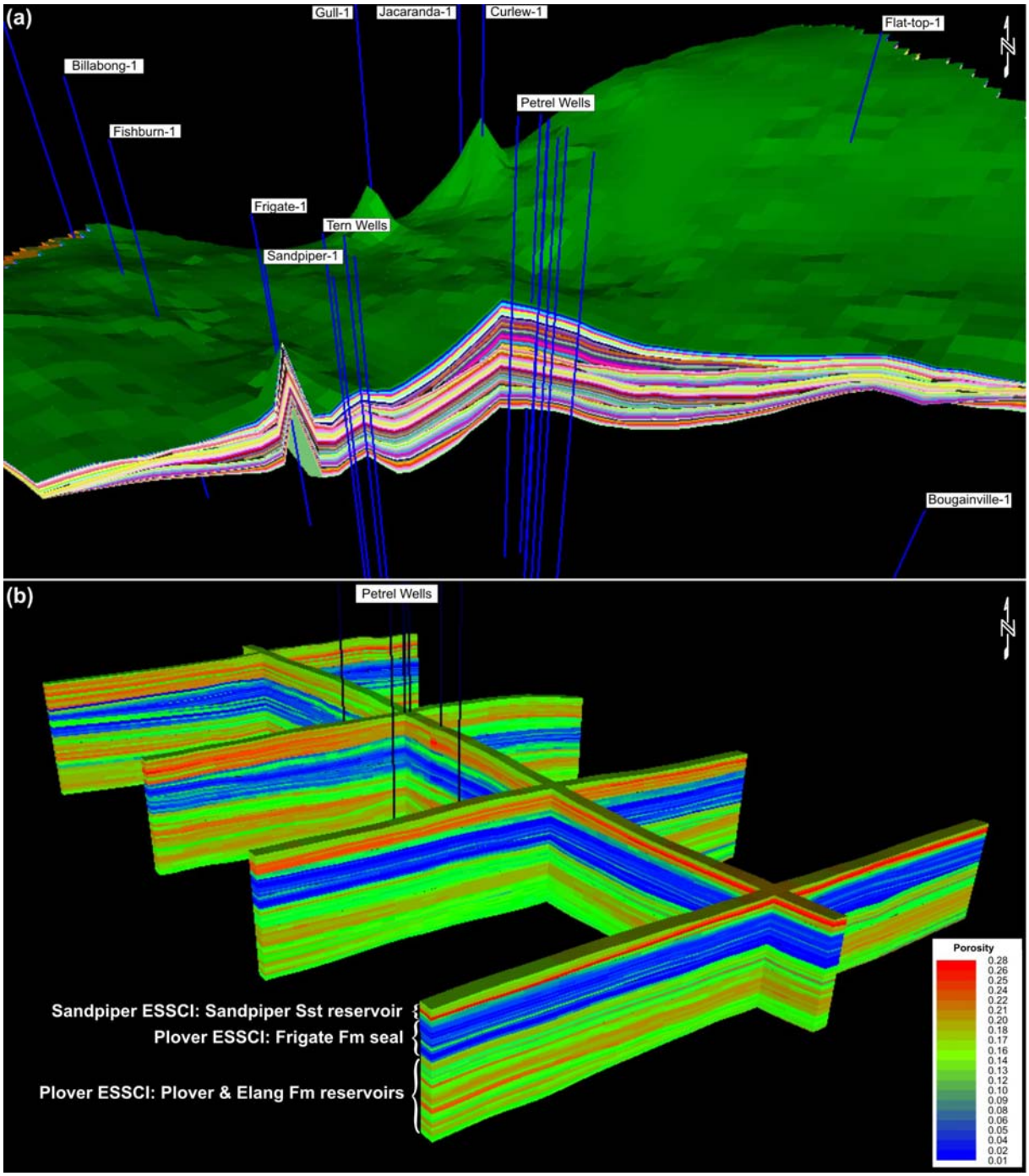

Figure 5.34 (a) Cut-away section through the regional-scale 3D geological model of the Petrel Sub-basin, showing layer distribution and geometries. (b) Fence diagram through the smaller 3D geological model (~80 x 40 km) over the Petrel Field and surrounding area, showing the geostatistical distribution of porosity.

accumulation around the injection well, the CO_2 is likely to rise to the top of the reservoir and spread out in thin layers beneath the Frigate Formation or Bathurst Island Group seals. The storage efficiency factors of DOE (2007) account for such factors as net to total area, net to gross thickness, effective to total porosity, areal displacement efficiency, vertical

displacement efficiency, gravity, and microscopic displacement efficiency. If these factors of 1–4 % are applied to the available pore volume, the potential storage capacity is still in the order of tens of thousands to hundreds of thousands of Mt of CO_2. Therefore, the potential CO_2 storage capacity of the Petrel Sub-basin Plover and Sandpiper ESSCIs is huge. A possible limitation to the amount of CO_2 that could actually be stored is the injectivity of the sandstones and the rate of injection that they can accommodate without significant over pressurisation.

Table 5.5 CO_2 storage capacity volumetric assessment for reservoir units within the Petrel Sub-basin ESSCIs.

Reservoir	Zone	Pore Volume (m^3)	Density (kg/m^3)	CO_2 (Mt)	Total CO_2 (Mt)	Total CO_2 (TCF)†	E = 1% CO_2 (Mt)	E = 4% CO_2 (Mt)
Sandpiper	Sandpiper Upper	1,370,000,000,000	600	822,000	1,206,600	22,738	12,066	48,264
	Sandpiper Lower	641,000,000,000	600	384,600				
Plover	Elang	3,290,000,000,000	600	1,974,000	3,630,000	68,406	36,300	145,200
	Plover Upper	1,200,000,000,000	600	720,000				
	Plover Lower	1,560,000,000,000	600	936,000				

† Conversion factor of 1 Mt = 0.018844539 TCF at standard temperatures and pressures (14.65 psia and 60ºF surface conditions).

5.9 POTENTIAL IMPACT ON EXISTING NATURAL RESOURCES

The existing hydrocarbon resources in the Petrel Sub-basin (the Petrel, Tern and Blacktip gas fields and the Barnett and Turtle oil fields) occur in much deeper reservoir units than the proposed ESSCIs. Therefore, these fields are unlikely to be compromised by CO_2 injection and storage. With regards to future hydrocarbon exploration, potential plays within the Mesozoic succession are very limited, as migration from the underlying Carboniferous and Permian source rocks is unlikely due to the presence of the Early Triassic Mount Goodwin Formation regional seal, and potential source rocks within the Mesozoic succession (such as the Frigate Formation) have been identified as poor quality source facies and of low maturity (McConachie *et al.*, 1995; McConachie *et al.*, 1996). Further hydrocarbon exploration is only likely to be focused within the stratigraphically deeper Carboniferous and Permian rocks.

5.10 CONCLUSIONS

Two stratigraphic intervals within the Jurassic–Cretaceous succession of the Petrel Sub-basin were assessed for their suitability for geological storage of CO_2. The detailed geological site characterisation process involved an interpretation of the geological structure, stratigraphic fill, reservoir and seal properties, petrography, geomechanics and hydrodynamics. The integration of all the various interpretations has yielded numerous results pertinent to the suitability of the Mesozoic succession in the Petrel Sub-basin as a potential site for geological storage of CO_2. The main outcomes are as follows:

- The structural geometry of the Jurassic–Cretaceous sediments is a simple slope: deepest in the northwest and sloping gently up-dip towards the southwest, south and southeast basin margins, with no structural closures (except for small anticlines above salt diapirs). Faulting intensity is low and is limited to the basin margins or in association with the salt diapirs.
- The stratigraphic fill reflects numerous relative sea level changes, exposing and flooding areas of the continental shelf. Eight unconformity-bound sequences were distinguished over the interval of interest, with clastic depositional environments ranging from predominantly fluvial at the base to fully marine at the top.
- The reservoir units of the Plover and Elang formations (Sequences 1 to 2) are characterised by thick (~450 m), laterally extensive (~85,000 km^2), braided fluvial to deltaic reservoir units, which are likely to have an overall excellent degree of interconnectivity. The overlying Sandpiper Sandstone reservoir (Sequences 5 to 6) is similarly laterally extensive, although not quite so thick (~200 m), and is characterised by shoreface to coastal plain sediments. The interconnectivity of these sediments depends on the degree of attachment of the shorelines, but is thought to be moderate to excellent considering the sand-prone nature of the interval.
- Reservoir quality is moderate to very good. The Plover/Elang formations have an average porosity of 19 % and permeability of 285 mD, whilst the Sandpiper Sandstone is slightly better quality with an average porosity of 22 % and permeability of 1675 mD. Therefore, the injectivity potential of both reservoir intervals is good. The quartz-rich mineralogy is unlikely to promote CO_2-water-rock interactions that could affect injectivity, although the possible migration of fine clay minerals during injection may potentially create localised reductions in reservoir quality.

- The Frigate Formation seal (Sequences 3 to 4) above the Plover/Elang formations is partially absent in the north of the basin and also exhibits a lateral facies change from marine shelf siltstones and shales in the basin centre to shoreface sandstones towards the south and east. Thus, communication between the Plover/Elang formations and the Sandpiper Sandstone is likely. However, the overlying Bathurst Island Group (Sequences 7 to 8) is a very thick (~700 m), regionally extensive (>85,000 km^2) marine shelf mudstone, which has good to excellent seal capacity (average CO_2 column height retention of 315 m). Therefore, the seal properties of the Bathurst Island Group are likely to provide secure containment.
- The likely migration pathway of CO_2 injected in a site along the axial trend of the basin is up-dip towards the southeast (southerly or easterly migration is also possible depending on the exact location of a potential injection site). The trapping mechanisms for the containment of CO_2 are not likely to be physical structural or stratigraphic traps, due to the lack of structural closure and increasingly sandier nature of the reservoir intervals towards the basin margins. However, as the potential migration pathways are long (e.g. ~100 km) and the *in situ* formation water velocity is very slow (1 cm/year), hydrodynamic trapping and associated residual and solubility trapping are likely be the dominant trapping mechanisms.
- Fault reactivation of the major northwest-trending basin-bounding faults is unlikely within the inferred stress regime. Faults of other orientations may possibly be able to reactivate if pressures are increased sufficiently, but most of these faults occur outside the potential CO_2 containment area.
- The potential CO_2 storage capacity is vast. Even if only 1 % of the available pore space was considered accessible, the potential storage capacity could still be in the order of thousands of Mt of CO_2.
- The existing hydrocarbon resources in the Petrel Sub-basin are unlikely to be compromised by CO_2 storage, due to their existence in much deeper reservoir units than the proposed CO_2 injection intervals.

In conclusion, the Petrel Sub-basin case study provides an example of CO_2 storage potential within a large-scale, saline formation with no defined structural closure. The geological site characterisation has determined that the proposed reservoirs are sufficiently porous and permeable to allow injection of supercritical CO_2, that the overlying Bathurst Island Group seal provides effective containment, and that its size is large enough to provide

more than enough storage capacity for any likely CO_2 source. Therefore, the Jurassic–Cretaceous succession in the Petrel Sub-basin is likely to be a suitable candidate for geological storage of CO_2.

The scale of potential storage capacity in deep saline formations is one of the main reasons why geological storage of CO_2 is considered to be a realistic solution to dealing with the large volumes of CO_2 being produced from the energy industries. Whilst the Petrel Sub-basin is presently a long way from sources of CO_2 and therefore may not be an economically realistic site for CO_2 storage, this study shows that basin-scale geological storage in comparable geological settings may provide a technical solution to the problem of reducing greenhouse gas emissions. If comparable sites can be located near significant point sources of CO_2 without interference to other resources, then the feasibility of geological storage of CO_2 in saline formations appears promising.